Title
DOMAIN HYPERFINE FIELDS IN SOME DILUTE FERROMAGNETIC ALLOYS STUDIED BY NMR ON ORIENTED NUCLEI

Author
Streater, Richard William.

Publication Date
1976-05-01

LBL-4981
c. 1

DOMAIN HYPERFINE FIELDS IN SOME DILUTE FERROMAGNETIC ALLOYS STUDIED BY NMR ON ORIENTED NUCLEI

Richard William Streater
(Ph. D. thesis)

May 1976

Prepared for the U. S. Energy Research and
Development Administration under Contract W-7405-ENG-48

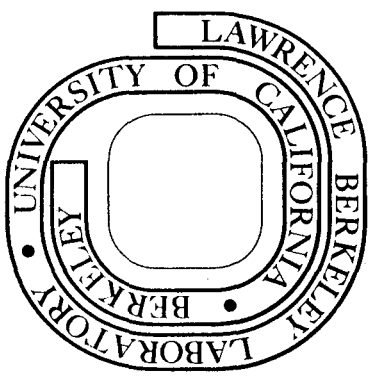

LBL-4981
c. 1

DISCLAIMER

DOMAIN HYPERFINE FIELDS IN SOME DILUTE FERROMAGNETIC ALLOYS
STUDIED BY NMR ON ORIENTED NUCLEI

Contents

DOMAIN HYPERFINE FIELDS IN SOME DILUTE FERROMAGNETIC ALLOYS STUDIED BY NMR ON ORIENTED NUCLEI

Richard William Streater

Materials and Molecular Research Division
Lawrence Berkeley Laboratory
University of California
Berkeley, California 94720

ABSTRACT

Hyperfine field distributions at the sites of ^{60}Co atoms dissolved in some dilute (up to 4%) CoFe and NiFe alloys have been measured by NMR on oriented nuclei at very low temperatures. The resonances are primarily in domains, and do not involve many of the uncertainties in line shape or poor resolution of other methods which have been used in the past. A method for preparing samples for high resolution nuclear orientation-NMR spectra is described.

The hyperfine field shifts due to neighboring impurities are shown to be consistent with a model in which the shifts are caused by moment perturbations in the neighboring shells surrounding an impurity, with RKKY-like spin density oscillations affecting the conduction electron and core polarization contributions to the hyperfine field. The observed shifts at a ^{60}Co site are +1.86±0.22 kG with a nearest neighbor substituent Co, -4.28±0.17 kG with a second nearest neighbor substituent, -3.41±0.07 kG for a third nearest neighbor substituent and -0.98±0.05 kG for a fourth nearest neighbor substituent. In the NiFe alloys, the shifts are -3.48±0.23 kG, -6.63±0.14 kG, -5.14±0.25 kG, and -1.49±0.14 kG respectively for Ni neighbors. The shifts are shown to be generally smaller than those at the Fe sites, the trends being consistent with a reduced number of itinerant electrons in going across the 3d transition

series and with the moment perturbations arising via the itinerant d's.

Small quadrupole contributions to the hyperfine interactions are shown to exist by the response in adiabatic fast passage resonance sweeps, but do not contribute significantly to the magnetic resonance lineshapes.

The ^{60}Co spin-lattice relaxation times have been measured for the main and satellite resonances in some CoFe alloys and no statistically significant changes in a function of alloy concentration or the sub-resonance excited were observed.

I. DILUTE FERROMAGNETIC ALLOYS

Hyperfine fields and moment distributions in dilute ferromagnetic alloys have been extensively studied by neutron diffraction,[1-5] cw NMR,[6-14] spin echo NMR[15-21] and Mössbauer spectroscopy.[22-30]

Spectra and moment distributions for most of the transition metals dissolved in Fe, both those which form local moments of their own, and those which do not, have been measured or inferred. The most studied case is that of Co in Fe, with the Fe sites being the object of most of the NMR and Mössbauer work.

In 1959, Gossard and Portis[31,32] observed strong nuclear resonance signals from ^{59}Co in pure Co metal, and there has been extensive use made of NMR to attempt to extract information regarding the electronic structure of ferromagnets. Soon after the discovery of ferromagnetically enhanced NMR, research on dilute alloys began. La Force et al.[6] and Koi et al.[7] observed mostly distinct, higher frequency satellites in the Co resonance in dilute Fe and Ni in Co alloys, which were attributed to impurities in neighboring shells about an Fe impurity.

Portis and Kanamori[33] noted that the intensities observed in the early work were considerably weaker than would be expected if the origin were indeed due to substituents in nearby positions, and proposed a model in which all the intensity was due to a near neighbor substituent only, and split by a dipolar field from the impurity and a pseudodipolar field due to the charge distribution in the neighboring d-shells.

Wertheim et al.[25] performed an analysis of the ^{57}Fe Mössbauer spectrum in Fe-based alloys and concluded that the magnitude of the changes in lineshapes with differing alloy concentrations must involve

at least N1 and N2 (i.e., nearest and next nearest neighbor) sites. Wilson[9] in 1964 studied CoFe and NiFe alloys by NMR and observed no satellites but showed resonance lineshapes broadened to low frequency which could not be rationalized with the Mössbauer spectra except by saying that the low resolution of the Mössbauer data precluded the observation of shifts due to neighbors farther than the first few shells. He felt that the NMR was sensitive to all the shells and that the net contribution was a reduction in the overall field due to interaction with many more distant neighbors.

The neutron scattering measurements by Collins and Low[1] of the magnetic moment perturbations around transition metal impurities in Fe had only very low resolution, thus allowing only an overall view of the magnetic defect structure in the alloys, but not permitting assignment of accurate moment values to the individual neighbors of an impurity. Campbell[2] obtained reasonably good agreement with the neutron scattering data with a very simple empirical model, assuming the hyperfine field arises from two contributions, one proportional to the local moment and one proportional to the average host moment. Using a simple band shape, Campbell and Gomès[4] developed a phenomenological model describing the scattering of degenerate electrons by impurity atoms (in terms of charge screening), based on Friedel's theory of alloys.[34,35]

Rubinstein et al.[15] published Mössbauer spectra for a series of low concentration Al, Si, and transition metal impurities in Fe and made an empirical fit to the data assuming a superposition of the hyperfine fields in the various occupational distributions of the

first three neighboring shells.

Detailed cw spectra of the Fe resonance in some dilute alloys were taken by Mendis and Anderson.[10-13] They concluded that, with the intensities they observed, they had seen satellites out to 4th or 5th nn although the intensity measurements were very difficult to correct for the base line. They did not assign any lines to N1 or N2 substituents and attributed this absence to large dipolar and pseudodipolar effects, causing broading to such an extent that the signal was lost in the baseline. In agreement with the Mössbauer work, they point out the validity of the assumption of additivity of impurity effects by noting a small satellite they assigned as due to two Co in the N3 shell with twice the frequency shift of the single substituent line. Figure I-1 shows the average field at the Fe sites as a function of Co concentration from Mössbauer studies and it can be seen that it is linear to about 20% Co, supporting this additivity idea.

By 1968, the basic experimental facts were still somewhat in question. Rubinstein[16] studied both the ^{59}Co and ^{57}Fe resonances by spin echo and cw NMR. He went through a fitting analysis similar to that of previous authors, assuming a random distribution of impurities, and, using his new intensity data, decided that the prominent satellite was a poorly resolved N1 and N2 doublet, claiming to resolve the 8:6 relative amplitudes due to the N1 and N2 substituents. He observed a marginally resolvable peak on the high frequency side of the main peak which was attributed to an N3 or N4 impurity.

Budnick[18,19] put some of the controversy into perspective with the observation that the integrated satellite intensities in his careful

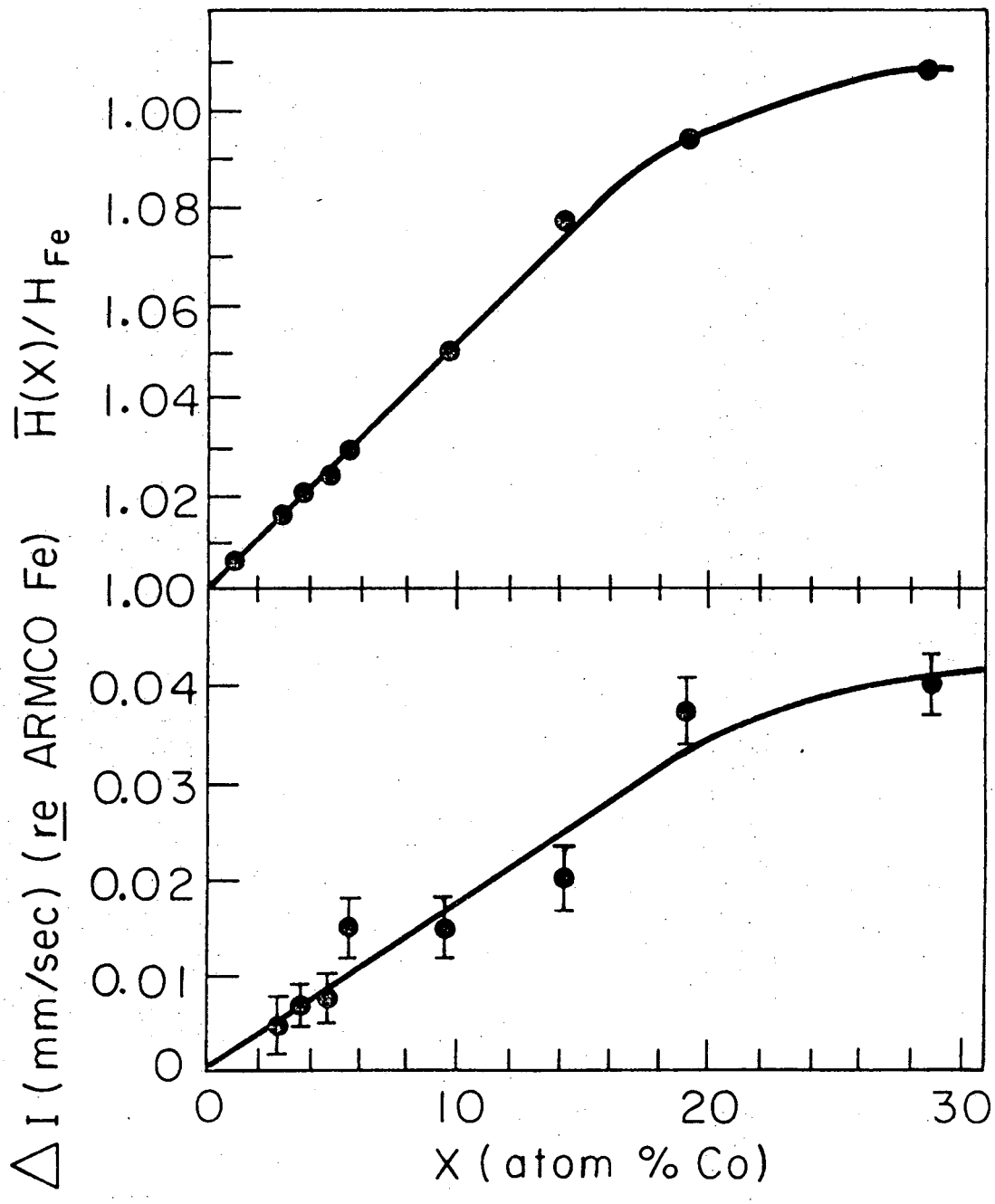

XBL 762-2281

Fig. I-1. Average hyperfine field at the Fe site as a function of Co concentration (from Ref. 43).

spin-echo measurements differed by as much as a factor of 1.5 or 2 from the intensities reported by Mendis and Anderson and Rubinstein, who measured only relative peak heights and did not consider line widths in matching intensities to the probability distributions. He showed that agreement with the neutron scattering results, which show mainly positive perturbed spin density leading to high frequency shifts in the MNR and Mössbauer spectra, could be obtained.

It might be pointed out that in many of the analyses, the amplitudes or heights of the various "sub-peaks" in the main satellite were compared with one another but apparently not to the main resonance to see if the assignments were at all reasonable in terms of the overall probability distributions.

Wertheim[26] criticized the analysis of Rubinstein and compared the magnitude of the shifts to some new Mössbauer data. He concluded that an N3 substituent gave a shift of 1.3% in agreement with Mendis and Anderson but also saw a very large (~3%) shift for N1 and a possible N2 nearby. He assumed all linewidths were the same and that a random statistical distribution obtained.

Stauss[20] proposed yet another model for the Fe and Co resonances in dilute CoFe alloys, taking into account the possibility that different widths might be associated with different lines due to dipolar broadening effects. His calculated spectra show reasonable agreement with some of the better experimental data, although two quite different sets of parameters seem to give fairly good matches to the Fe spectra.

There are experimental difficulties associated with all the

techniques used in the studies mentioned here. The poor spatial resolution of the neutron scattering data does not permit assignment of moments to the individual sites neighboring the impurity. The Mössbauer spectra do not in general have sufficient resolution to allow the observation of distinct satellites at all, and usually only a broadening and shift of the outer lines can be observed. The NMR experiments rely on enhancement by domain wall motion. The averaging of the B_1 with the local magnetization, the variation of the enhancement factors across the domain wall, and the consequences of the domain walls consisting of area segments of different sizes, which are immobile at their perimeters, must all be considered.[36,37] The position of the resonant nucleus with respect to the wall, the power applied, and the methods of applying the rf all introduce variables which may not be fully accounted for.[38] Butler[39] suggested that single fast passage experiments might permit relative intensities to be used in identifying the sites, but showed that for anisotropic hyperfine fields such as in hexagonal Co or for near neighbors to an impurity, the signal is drastically modified by the anisotropic hyperfine fields and enhancement mechanisms.

Vincze and Campbell[28] did an extensive serier of Mossbauer experiments on all the transition metals soluble in Fe and performed a very careful, detailed analysis of the spectra, including all six Mossbauer lines in their fits, not just the outer ones as had been done in the past. They showed quantitatively that the behavior of the <u>average</u> hyperfine field changes due to impurities could be given, as before, in terms of a core polarization proportional to the d moment

on a particular site and a non-localized conduction electron polarization term. By including the value of the impurity hyperfine field they showed

$$\frac{d\bar{H}}{dc} + (H_i - H_{Fe}) = \left(\frac{H}{\mu}\right)_{\text{pure Fe}} \cdot \frac{d\bar{\mu}}{dc} \qquad \text{(I-1)}$$

for 3d impurities, where $d\bar{\mu}/dc$ is the change in average magnetization of the alloy per substituted impurity atom. They gave a general expression for the total change in neighbor site fields with terms involving d moment changes on the Fe sites as well as the effect of the conduction electrons at the Fe sites due to the moment changes at the impurity site.

Along similar lines, Stearns[40] has developed a semi-quantitative model of the origin of the hyperfine fields at the solute atoms in Fe, considering both RKKY type interactions where the spin density of the itinerant electrons arises from a Coulomb exchange interaction between the localized and itinerant electrons (yielding a positive CEP spin polarization) and an effective exchange interaction through interband mixing of the conduction and local moment orbitals (yielding in most cases a negative CEP). She shows that an RKKY-like radially oscillatory hyperfine field shift can result from a consideration of these aspects. Details of these methods may be found in review articles by Blandin[41] and Narath[42] and references cited therein.

An extension of the model to moment distributions and hyperfine fields at, and surrounding, transition metal solute atoms in Fe and in dilute alloys has been developed.[43-45]

Assuming each atom of the lattice causes a CEP oscillation around it, that for dilute alloys, these oscillations may be superimposed, and that the solute atom goes into the matrix with a perturbation that can be represented by an increase in the moment of the Fe atoms surrounding the solute, use may be made of the average saturation moment of dilute CoFe alloys[46,47] to calculate the hyperfine field shifts. It can be shown that, from the average saturation moments of the dilute alloys, considering the first 6 shells

$$0.47\mu_{Fe} = -\mu_{Fe} + \sum_{n=1}^{6} M_n \Delta\mu_n + \mu_{Co} \qquad \text{(I-2)}$$

where M_n is the number of sites in the n^{th} shell and $\Delta\mu_n$ is the increased moment in the n^{th} shell surrounding a Co impurity. A functional variation of the form

$$\Delta\mu_n = \Delta\mu_1 \left(\frac{r_1}{r_n}\right)^m$$

is used, where $\Delta\mu_1$ is the moment increase on the Fe atoms in the first neighbor shell and the exponent, m, is the radial dependence of the moment perturbations.

In the usual manner,[48,52] the hyperfine field at the Fe atom is given by

$$H_{Fe} = H_{cp} + H_{cep} \qquad \text{(I-3)}$$

where H_{cp} is the field due to core polarization and H_{cep} is due to conduction electron polarization. The H_{cep} term can be broken up into two contributions, H_s, due to the Fe atom itself and H_Σ due to all the surrounding atoms.

$$H_{Fe} = H_{cp} + H_s + H_\Sigma \qquad \text{(I-4)}$$

The first two terms, due to the moment on the Fe itself can be combined as H_M. H_Σ for pure iron has been measured and so H_M can be calculated.

$$H_M = H_{cp} + H_s = H_{hf} - H_\Sigma = -346 + 145 = -201 \text{ kG} \qquad \text{(I-5)}$$

or 90.5 kG/μ_B. The CEP hff shifts in the n^{th} shell, ΔH_n in iron were obtained from shifts in FeSi and FeAl alloys[53] and are -12.1 kG/μ_B for the N1 shell, -2.7 for N2, +2.4 for N3, +0.6 for N4, +0.3 for N5 and +0.6 for N6. The occupational distribution surrounding a solute atom, is given by Stearns[43] in her Table II, part of which is reproduced here for the first nearest neighbor to a Co, in Table I-1. For example, consider the Fe which is first nearest neighbor to a Co. Three of its Fe nn are N2 to the Co, 3 are N3 and one is N5. In the N2 shell, three Fe are N1 to the Co and three are N4, and so on. The hyperfine field shift on an Fe in the n^{th} shell to a Co is the sum of the shifts due to the moment change on the Fe itself plus the change in the CEP due to neighboring moment changes, including the impurity atom itself. For the Fe^1 atom, i.e., N1 to a Co, then,

$$\begin{aligned} H_{Fe}^{N1} = &-90.5(\Delta\mu_1) - 12.1(\mu_{Co} - \mu_{Fe}) \\ &-12.1(3\Delta\mu_2) + 3\Delta\mu_3 + \Delta\mu_5) \\ &- 2.7(3\Delta\mu_1 + 3\Delta\mu_4) \\ &+ 2.4(3\Delta\mu_1 + 6\Delta\mu_4) \\ &+ 0.6(3\Delta\mu_2 + 6\Delta\mu_3 + 3\Delta\mu_5 + 3\Delta\mu_6) \end{aligned} \qquad \text{(I-6)}$$

Table I-1. Occupational distribution of the atoms surrounding an Fe atom which is nearest neighbor to an impurity.

N1 Shell	Nn(imp)	N2 Shell	Nn(imp)	N3 Shell	Nn(imp)	N4 Shell	Nn(imp)
1 Co		3 Fe	N1	3 Fe	N1	3 Fe	N2
3 Fe	N2	3 Fe	N4	6 Fe	N4	6 Fe	N3
3 Fe	N3			3 Fe	N7	3 Fe	N5
1 Fe	N5					3 Fe	N6
						6 Fe	N8
						3 Fe	N9

Similar expressions can be worked out for the hyperfine shifts for Fe sites more distant from the Co impurity. Based on this model, spectra were calculated varying the exponent, m (= 2, 3, 4) for the moment perturbation, and varying μ_{Co}. Only $1/r^3$ moment perturbations match the experimental spin-echo spectra at all and a value of $\mu_{Co} = 1.9$ gives good agreement and is a very reasonable value.[1,52]

For a $1/r^3$ moment perturbation, the expressions are:

$$\Delta H_{Fe}^{N1} = -121.6\ \Delta\mu_1 - 12.1(\mu_{Co} - \mu_{Fe}) \qquad \text{(I-7a)}$$

$$\Delta H_{Fe}^{N2} = -106.2\ \Delta\mu_1 - 2.7(\mu_{Co} - \mu_{Fe}) \qquad \text{(I-7b)}$$

$$\Delta H_{Fe}^{N3} = -50.6\ \Delta\mu_1 + 2.4(\mu_{Co} - \mu_{Fe}) \qquad \text{(I-7c)}$$

$$\Delta H_{Fe}^{N4} = -25.1\ \Delta\mu_1 + 0.6(\mu_{Co} - \mu_{Fe}) \qquad \text{(I-7d)}$$

$\Delta\mu_1$ is obtained from Eq. (I-2) using $\mu_{Co} = 1.9\ \mu_B$

This model seems to work quite well with the hyperfine fields at the Fe sites. The consideration of the fields at impurity sites with neighboring impurities is of course a much more difficult problem. The model requires dilute alloys, that is, only one impurity in the surrounding shells to allow the approximations to hold, even though the additivity assumption seems to be valid up to much higher concentrations. It can be used to calculate the hyperfine fields at the impurity sites in terms of the sum of CEP and CP contributions, which can be derived independently only if the impurity is extremely dilute. The effect of having a second impurity in the shells neighboring an impurity itself is very difficult to determine because of the synergistic effects of each of the impurities affecting the moment

distribution in the Fe lattice, on each other, etc. In order to even begin to approach the problem in a fundamental theoretical way, it was felt that an independent, high resolution, unambiguous determination of the hyperfine field shifts at the impurity sites due to neighbor impurities was required. Thus the present work, utilizing the method of NMR on oriented nuclei, which gave promise of providing spectra amenable to such an analysis was undertaken. The resonances are primarily in domains and are not seriously affected by the wall motion. The technique is extremely sensitive and allows the spectra to be taken on very dilute impurities as easily as the more concentrated samples. With careful sample preparation, it was felt that the resolution could be made comparable to or better than that of the best spin-echo spectra for the dilute alloys. A very simple way of parameterizing the shifts based on the data and an extension of the model to the impurity sites will be given in Section IV.

II. NMR ON ORIENTED NUCLEI

A. Nuclear Orientation

Thermal equilibrium nuclear orientation is achieved by coupling the nuclear spin system to a fixed spatial direction by electric or magnetic fields. The substates of energy E_m have different populations given by a Boltzmann distribution function, and at temperatures where $(E_m - E_{m+1})/kT$ is $\cong 1$, a degree of nuclear orientation results.

Several methods of achieving the required energy splitting are used, including the "brute force method",[54] requiring high external magnetic fields; the use of hyperfine splittings in paramagnetic ions;[55-57] and the alignment of electronic spins which produces large internal fields in ferro- and antiferromagnets.[58,59] The thorough review article of Blin-Stoyle and Grace[60] develops the theory of these methods in some depth and the interested reader is referred to the article for detailed information. Introductions to these and other dynamic methods of achieving nuclear orientation, including experimental considerations are given in books and review articles by Daniels,[61] Jeffries,[62] Shirley,[63] and Lounasmaa,[64] among others.

For the case at hand, ^{60}Co in iron and iron alloys, the magnetic Zeeman interaction is used to effect the population distribution at very low temperatures achieved by adiabatic demagnetization of a paramagnetic salt. The Hamiltonian for this system can be simply represented as

$$\mathcal{H} = -\vec{\mu}\cdot\vec{H} \qquad \text{(II-1)}$$

where $\vec{\mu}$ is the nuclear magnetic moment and $\vec{H}$ is the effective field at the nucleus.

The 2I + 1 spin degeneracy is lifted and the probability of a given state being occupied in an ensemble of nuclei in thermal equilibrium is given by the Boltzmann distribution function

$$P(m) = \frac{\exp(-mg\mu_N H/kT)}{\sum_m \exp(-mg\mu_N H/kT)} \qquad \text{(II-2)}$$

For ^{60}Co in Fe, the hyperfine interaction is less than 10 mK, so temperatures of this order are required to obtain a significantly unequal population distribution.

The γ ray angular distribution function for an ensemble of thermally oriented radioactive nuclei is given by

$$W(\theta) = 1 + \sum_{k\,\text{even}}^{k\,\text{max}} B_k U_k F_k Q_k P_k(\cos\theta) \qquad \text{(II-3)}$$

where $W(\theta)$ is the intensity of radiation at angle θ between the quantization axis and the direction of the observed emitted radiation. The sum is over even terms only, for parity conserving γ transitions. $P_k(\cos\theta)$ are the Legendre polynomials.

The B_k's are the orientation parameters and contain all the information regarding the temperature, hyperfine field, and other external parameters.

$$B_k = [(2I + 1)(2k + 1)]^{1/2} \sum_m (-1)^{I-m} \begin{pmatrix} I & I & k \\ m & -m & 0 \end{pmatrix} P(m) \qquad \text{(II-4)}$$

The U_k's are angular momentum deorientation parameters associated with unobserved preceding transitions. They act as an attenuating factor in the product and are identical to those used in angular correlation measurements.

$$U_k = [(2I_i + 1)(2I + 1)]^{1/2} (-1)^{I_i+I-L} \begin{Bmatrix} I_i & I_i & k \\ I & I & L \end{Bmatrix} \qquad \text{(II-5)}$$

For more than one preceding transition, the final U_k is the product of the individual U_k's for each transition.

The F_k's are the angular distribution coefficients, again as used in angular correlation theory. For single multipolarity γ-rays

$$F_k(LLII_i) =$$

$$(-1)^{I+I_i-1} [(2k + 1)(2I_i + 1)]^{1/2} (2L+1) \begin{pmatrix} L & L & k \\ 1 & -1 & 0 \end{pmatrix} \begin{Bmatrix} L & L & k \\ I_i & I_i & I \end{Bmatrix} \qquad \text{(II-6)}$$

These coefficients have been tabulated in several places,[65,66] the most convenient of which is a paper by Krane.[67]

The upper index, k_{max} is determined by the spins of the nuclear levels and by the multipolarity of the radiations. For initial state I_i, $k \leq 2I_i$ for the B_k. For transitions from I_i to I, of multipolarity L, the F_k vanish for $k > 2I_i$ or $k > 2L$. Thus for multipole order $L \leq 2$, which is generally the case, only the $k = 2$ and $k = 4$ terms need be considered for γ transitions.

Since the radiation detector subtends a finite solid angle, an additional correction for this attenuation must be made. The solid angle correction factors, Q_k, have been tabulated for solid state and NaI detectors of various sizes and distances from the source.[68,69]

The decay scheme for ^{60}Co is given in Fig. II-1. The hyperfine field is -287.7 kG in Fe and the nuclear moment is 3.754 nuclear magnetons. The hyperfine splitting is thus 7.96 mK. The calculated anisotropy vs temperature curve is shown in Fig. II-2.

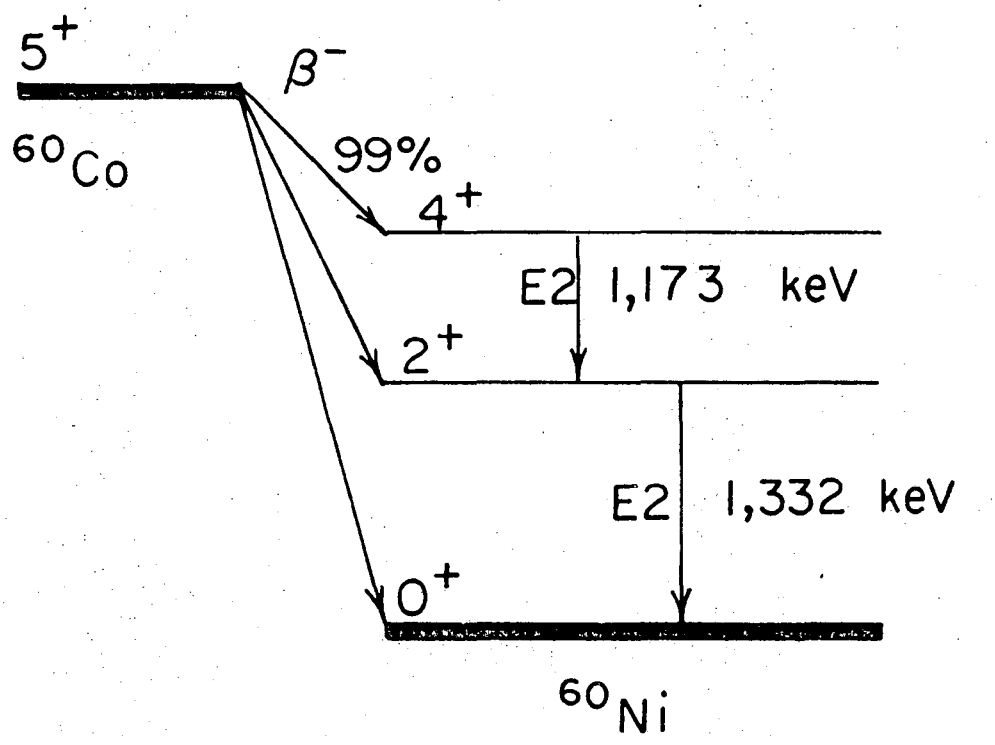

Fig. II-1. ^{60}Co decay scheme.

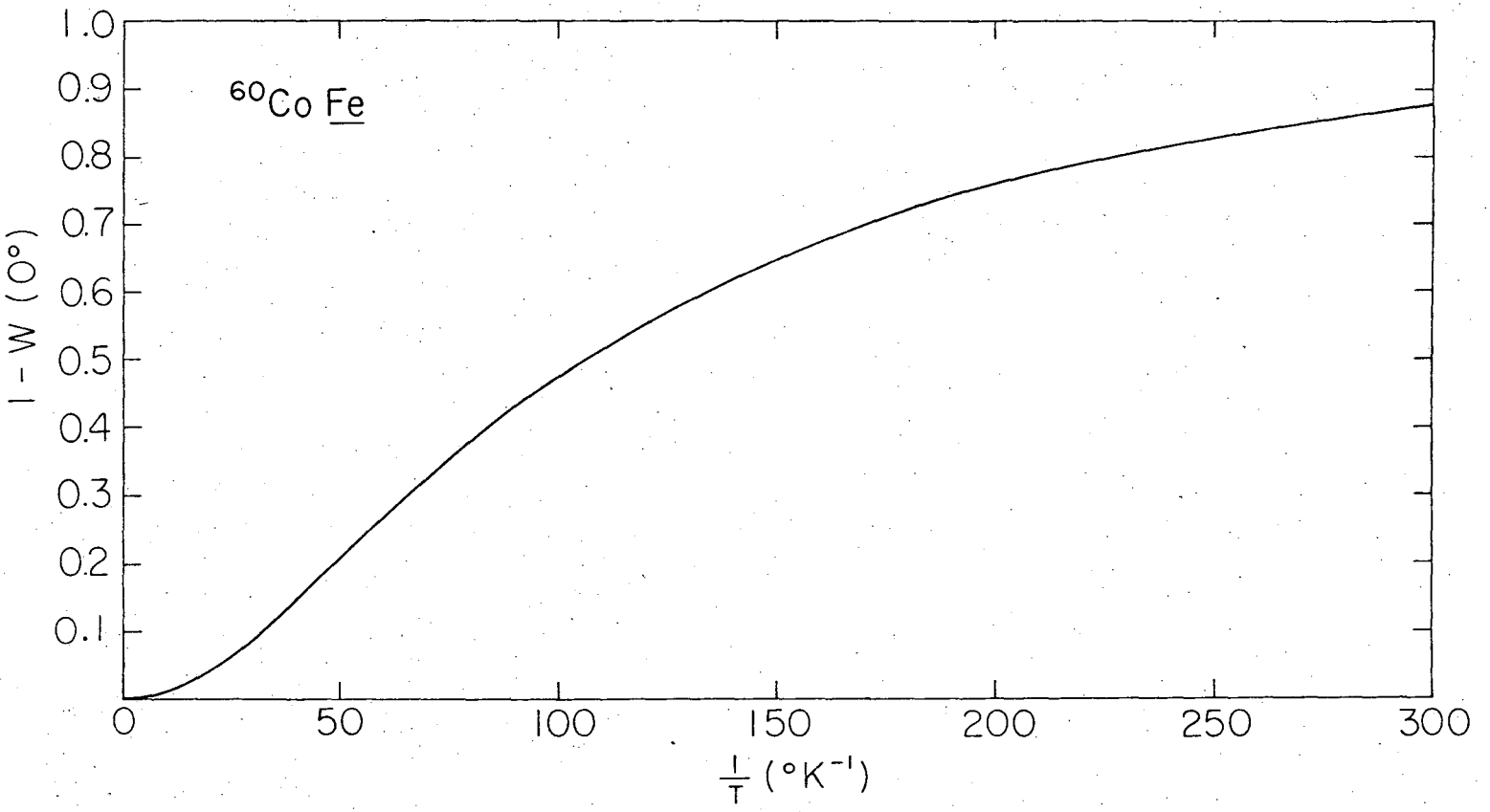

Fig. II-2. γ-ray anisotropy for ^{60}Co in Fe.

B. NMR on Oriented Nuclei

The theory of NMR is well established and its application to ensembles or oriented nuclei, developed in the late 1960's has been fully discussed in the literature.[70-74] NMR in ferromagnets has been discussed, for example in review articles by Portis and Lindquist[75] and Budnick.[76] A full, rigorous and extensive treatment of radiative detection of NMR in all its glory has been given by Matthias et al.[77] Only certain concepts germane to the experiments described herein will be mentioned.

The effective field at the nucleus in ferromagnetic lattice can be written as

$$H_{eff} = H_{hf}^{o} + H_L + H_{app} - DM \qquad (II-7)$$

where H_{hf}^{o} is the hyperfine field, H_L is the Lorentz field, H_{app} is the applied external field and DM is the demagnetizing field. Generally an effective hff

$$H_{hf}^{eff} = H_{hf}^{o} + H_L \qquad (II-8)$$

is reported and the magnetizing field inside the sample is H_{app} - DM.

As in conventional NMR, we can consider a system with a magnetic moment $\vec{\mu} = \gamma\vec{I}$, a static field $\vec{H}_o$ along the z axis and an oscillatory field $\vec{H}_1(t) = 2\vec{H}_1\cos\omega t$ along the x axis. The motion of $\vec{\mu}$ follows the torque equation

$$\frac{d\vec{\mu}}{dt} = \gamma\vec{\mu}x\vec{H}_o \qquad (II-9)$$

precessing around H_o with frequency $\omega_o = \gamma H_o$. Transforming into the Larmor frame, H_o disappears and $\vec{\mu}$ no longer precesses about the z axis. The oscillatory field may be resolved into its left and right circularly polarized components, and the component with the correct sense in the Larmor frame will be a constant field along the x axis. The resonance is understood as a precession about this H_1 field through an angle $\sim\pi/2$, inducing transitions between $|m\rangle$ levels. The resonance is observed as a partial destruction of the γ-ray anisotropy due to the disruption of the thermal equilibrium population distribution, monitored as a function of rf frequency. The power requirements for causing sufficient transitions to create an observable reduction in the anisotropy are such that H_1 must be sufficiently large that $\omega_1\tau_c \cong 1$, where $\omega_1 = \gamma H_1$ and τ_c is the correlation time T_1 or $T_{1/2}$.

H_1 at the nucleus is enhanced by the hyperfine enhancement factor, η,

$$\eta = 1 + H_{hf}/H_{app} \qquad \text{(II-10)}$$

since the electron magnetization can follow the rf and acts on the nucleus via contact interactions. Thus

$$H_1^{eff} = \eta H_1^{app} = (1 + H_{hf}/H_{app})\, H_1^{app} \qquad \text{(II-11)}$$

The natural linewidth $\lambda \cong 1/T_2 \cong 10^{-2}$ Hz is not attainable and inhomogeneous broadening normally results in linewidths of the order 10^6 Hz. At any one time, the rf induces transitions only within a bandwidth λ and the rf must be modulated over a much larger bandwidth, at a rate faster than T_1, thereby involving many spin packets of

width $\sim 1/T_2$ in order to have an observable resonant destruction of anisotropy. Various considerations of modulation frequency, width, power requirements, etc, have been discussed by Barclay.[78]

Fortunately, the enhancement is just sufficient in many cases to allow the experiment to be performed at external rf power levels (mG) which do not cause excessive eddy-current heating of the cooled sample and other parts of the cooling apparatus. Of course, in the attempts to resolve satellites in the alloy spectra in this study, the modulation width had to be kept below the inhomogeneously broadened linewidths, otherwise details of the spectra would have been lost.

III. EXPERIMENTAL

The demagnetization cryostat (see Fig. III-1) and rf system were similar to those used previously in this laboratory,[78-80] with certain modifications in design and technique which will be discussed below.

A. Dewars

The helium dewars consisted of an outer 10 in. diameter aluminum tube for the 4° bath, separated from the inner 1° bath (4-1/2 in. dia) by a vacuum space. The outer vacuum jacket contained layers of aluminized mylar "superinsulation" to reduce the heat leak from room temperature, as no liquid nitrogen bath was used. The 1° bath was pumped down to a pressure of 30 to 100μ (less than 1K) by a 1250 cfm Kinney booster pump.

B. Cryostat

The cryostat itself consisted of the pill container constructed from 0.035 in. wall stainless steel tube, 10 in. long with upper and lower flanges permitting super-leak-tight connection to the 1-1/2 in. pumping tube above and to a removable tailpiece below. Radiation baffles were soldered inside the pumping tube just above the pill top flange and at a point about half way up. One-sixteenth in. indium wire O-rings were used for both the 4 in. top flange and for the 3/4 in. flange at the tailpiece. Care must be exercised in the construction of the O-rings from the wire, and the use of a torque wrench (20 in.-lb on 6-32 hex head screws and 30 in.-lb on 8-32) ensures that even and consistent pressure is applied all around. Not a single leak was encountered in over 3 years of work, involving dozens of cyclings to room temperature for disassembly and reassembly for sample changing

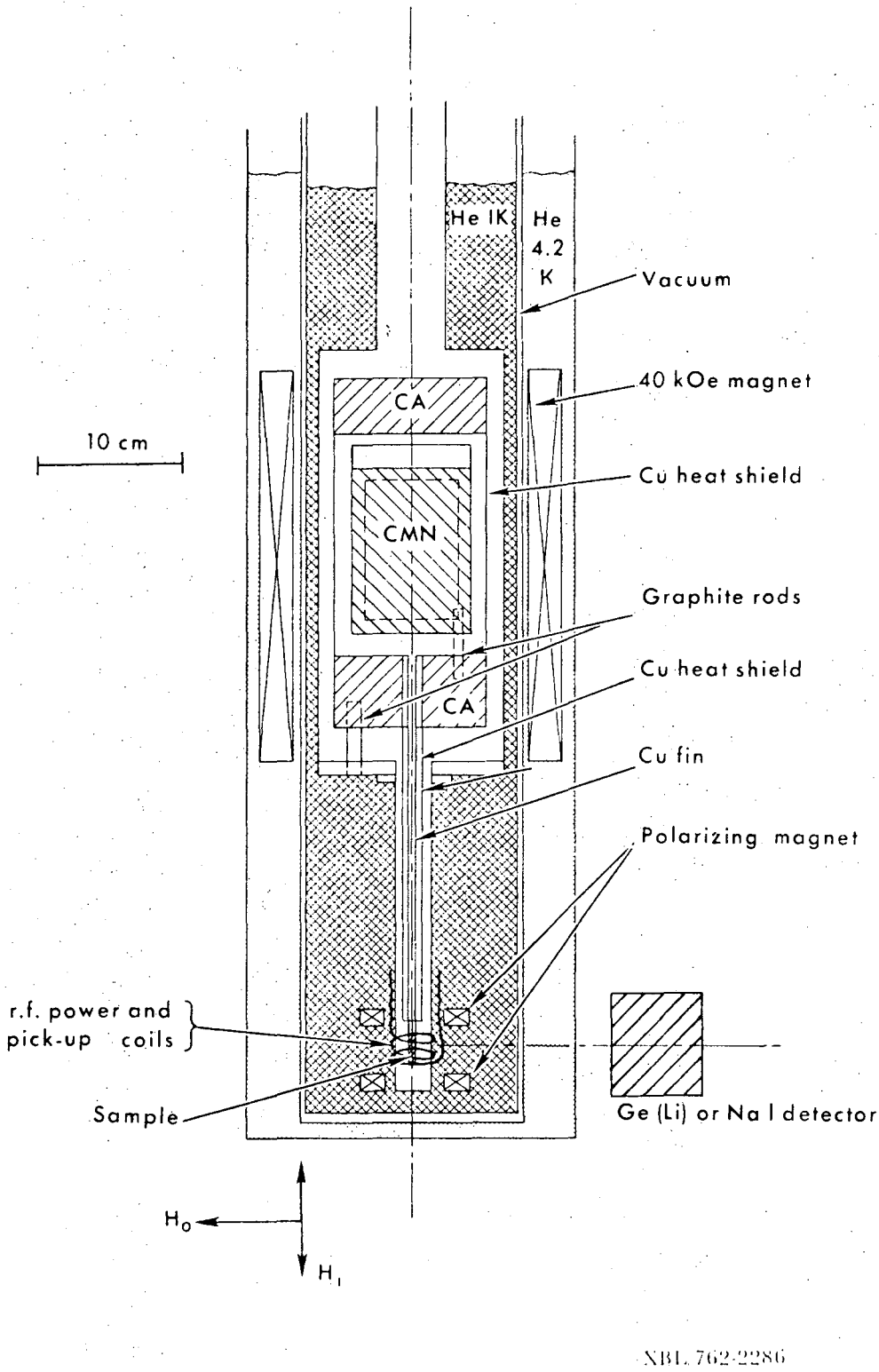

Fig. III-1. Dewar and cryostat-schematic.

and repair. The tailpiece had a Kovar to pyrex graded seal, with the bottom section being glass to allow the rf to penetrate to the sample.

C. Magnets

The main cooling solenoid was suspended in the 4° bath and was normally run at I = 105 amps (calibrated 363 gauss/amp). It could be raised by a block and tackle arrangement after completion of the demagnetization to reduce the residual fields (locally up to several hundred gauss) from the region around the pill and to reduce interference with the photo-multiplier tubes in the detectors. The polarizing magnet, a superconducting pair, was mounted on the bottom of the cryostat in the 1° bath and could be charged to a maximum of 20 amps (200 gauss/amp).

D. Pill Assembly

The pill (Fig. III-2) consisted of three major parts: (i) an upper $CrK(SO_4)_2 \cdot 12\ H_2O$ (CKA) guard pill with an annealed ETP 0.005 in. copper outer cylinder with contact fins embedded in the slurry. The cylinder extended down around the outside of the main cooling pill and acted as a heat shield and cryopump for residual gases during demagnetization. The top cover and base insert were machined from 1/4 in. NEMA G-10 epoxy-fiberglass.

(ii) The central $Ce_2Mg_3(NO_3)_{12} \cdot 24\ H_2O$ (CMN) cooling pill made from mylar and NEMA. Twenty 0.005 in. Cu fins tapering to a silver soldered stalk passing through the bottom were embedded in the slurry, providing indirect thermal contact for cooling the sample.

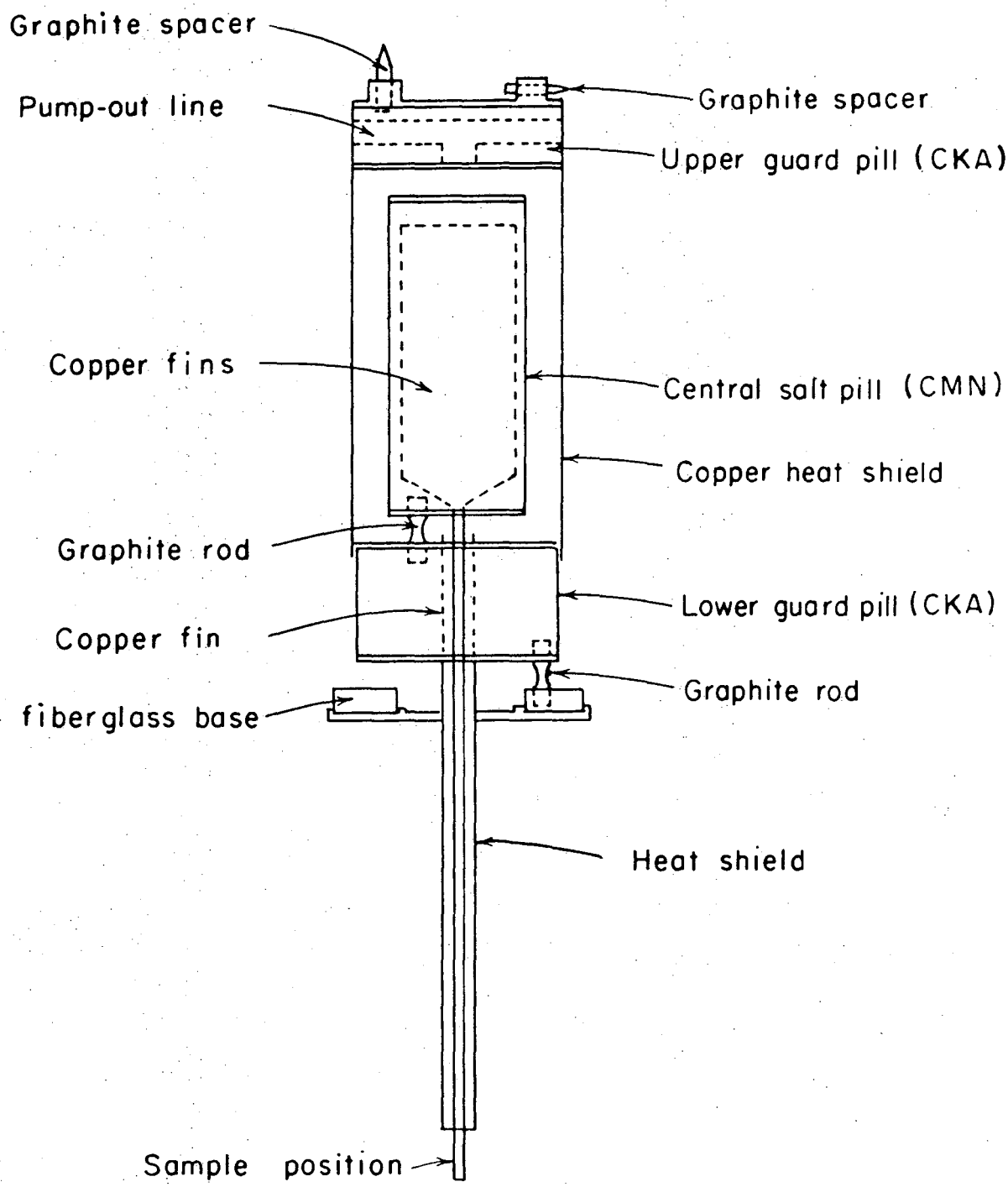

Fig. III-2. Cooling pill--detail.

(iii) The lower CKA guard and support pill with a copper foil tube extending through the bottom, acting as a heat shield for the inner cooling stalk.

The slurries were made from freshly prepared crystals of the salts, ground in a ball mill and sifted, using only those particles passing through #50 screen for CMN and #30 screen in the case of CKA, and mixing to the consistency of a stiff paste with glycerol (for CMN) or a 50:50 mixture of gycerol and saturated aqueous solution of the salt (for CKA). All joints in the slurry containers were made leak tight with Shell Epon 828 resin and Versamid 125 Catalyst. The support legs and spacers were made from 1/4 in. diameter ATJ or YU-60 graphite rods, reduced in diameter with the middle to 1/8 in. The slurries were replaced several times during the course of the experiments since they tend to degrade slightly after many thermal cyclings.

Thirty μ of ^{3}He was used as exchange gas to provide initial thermal contact between the 1° bath and the salt pills. This permits very quick pumpouts and the expense is quite minimal as only a few cc-atmospheres are required for each run.

E. Rf System

Rf power at the sample position was provided by a 2 turn coil of #24 Cu wire embedded in a support formed of casting resin which fit snugly around the glass tailpiece at the level of the sample. Immediately adjacent to the power coil was a similar pick-up coil used to monitor the rf level at the sample. The relation between H_1 at the sample and the field measured by the pick-up coil was calibrated using a small probe coil prior to assembly of the apparatus.

A schematic of the system is shown in Fig. III-3. A Willtron 610-B rf generator providing ~1 volt (peak-to-peak) with internal frequency modulation, was modified to allow greater sensitivity in the FM bandwidth settings and to permit the frequency to be swept by an external slow speed motor and gear box arrangement. A Hewlett Packard 5245L electronic counter with 5253B frequency converter was used to monitor the carrier frequency and to check the FM bandwidths. Normally a field of about 1 to 10 mG (p-p) was applied with an FM bandwidth of from 150 to 500 kHz, sawtooth modulated at 100 Hz. Low concentration spectra used a narrow modulation width, giving good resolution with good statistics, while higher widths were necessary to improve the signal to background ratio in the more concentrated samples.

The signal applied from the oscillator (through an amplifier or attenuator) and the signal from the pick-up coil were monitored on a Tektronix 661 Oscilloscope with 4S1 dual trace sampling unit and 5T3 timing unit. The pickup and power coils were connected by gold-plated pin plugs to 0.141 in. stainless steel semi-rigid 50 ohm co-ax, specially made with a silver coated stainless steel conductor instead of the normal Cu. This reduced the heat leak to the 1° bath considerably and allowed lower bath pressures to be achieved. The leads passed through vacuum feed-throughs on the top flange of the cryostat and, external to the apparatus, 1/2 in. Superflexible Heliax cable type FSJ4-50 was used. The entire dewar and pumping system was grounded by 4/0 Cu cable to the main electronics rack bus-bar which was directly connected to a ground pad, buried outside the building. During resonance runs the rf generator, frequency counter and sampling scope were floated

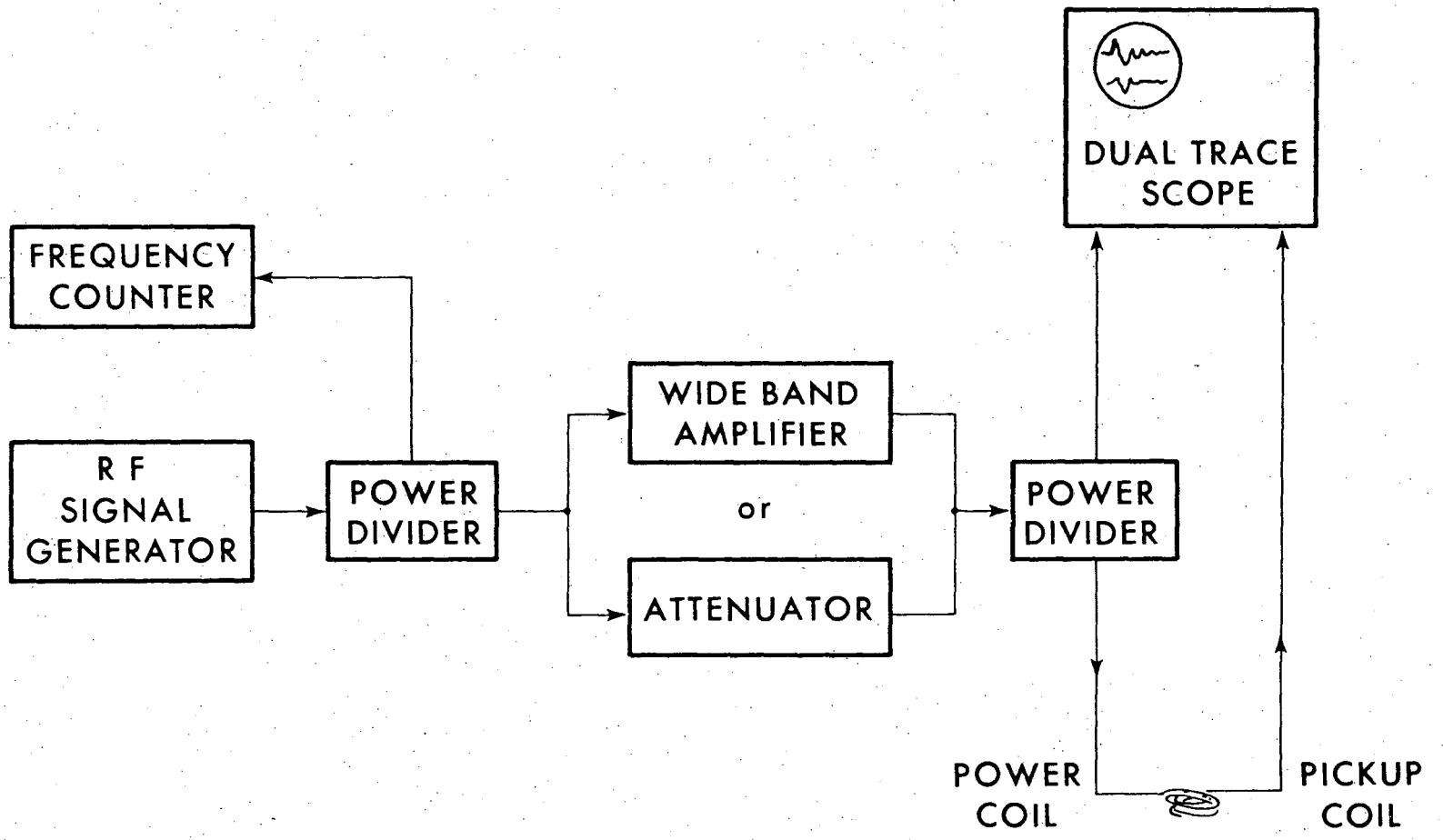

Fig. III-3. R.f. system--schematic.

XBL 763-2507

from the normal ground and grounding of the entire rf system was achieved solely through the rf cable shields. This system and these precautions allowed excellent performance with no significant power resonances in the frequency range of interest in the coils chosen for use in the experiments. With construction of suitable coils, it would be possible to use the arrangement for frequencies up to 1 GHz or more. No degradation of the sinusoidal waveform was apparent as shown in Fig. III-4 for 150 and 500 MHz.

During a resonance run, the frequency was swept slowly through the resonance region at a rate of about 3 MHz per hour as a multiscaler accumulated ^{60}Co γ-ray anisotropies as a function of frequency.

F. γ-Ray Counting System

Shown schematically in Fig. III-5 is the electronics system used for the NMR/ON experiments. Signals from a 3 in.×3 in. NaI detector located at 0° or 90° with respect to the polarizing field were pre-amplified and sent to a high rate linear amplifier. The single channel analyzer window was open to both the 1173 and 1332 keV γ's since they both have the same anisotropy and counts from both peaks could be used. A Packard model 16 or TMC model 1001 was used in multiscaling mode to accumulate counts in order to monitor the temperature and to accumulate the resonance spectrum. In some instances the entire γ-spectrum counts were stored in the multiscaler as a function of frequency, or the full spectrum recorded using an ADC with a PDP-7 computer and stored on magnetic tape for subsequent analysis.

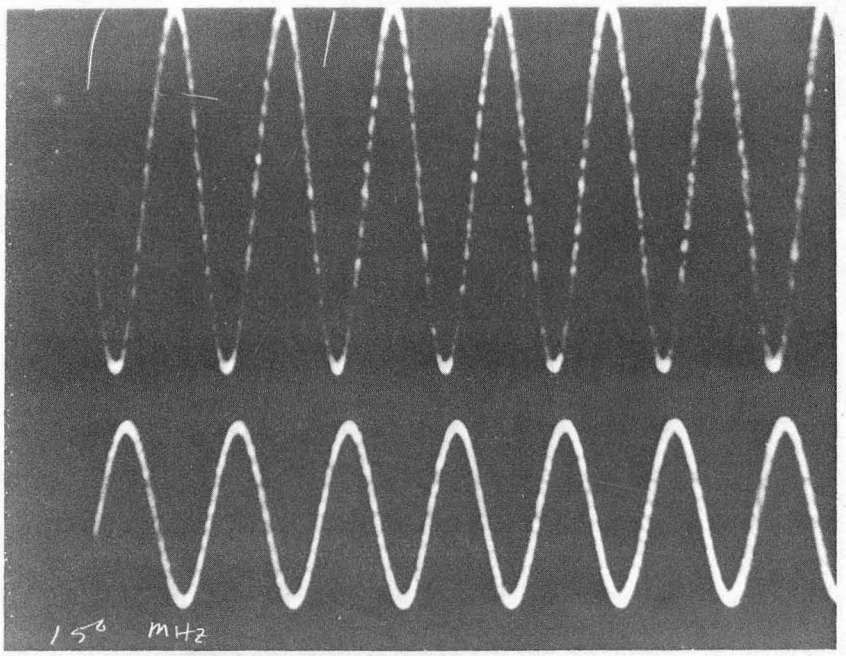

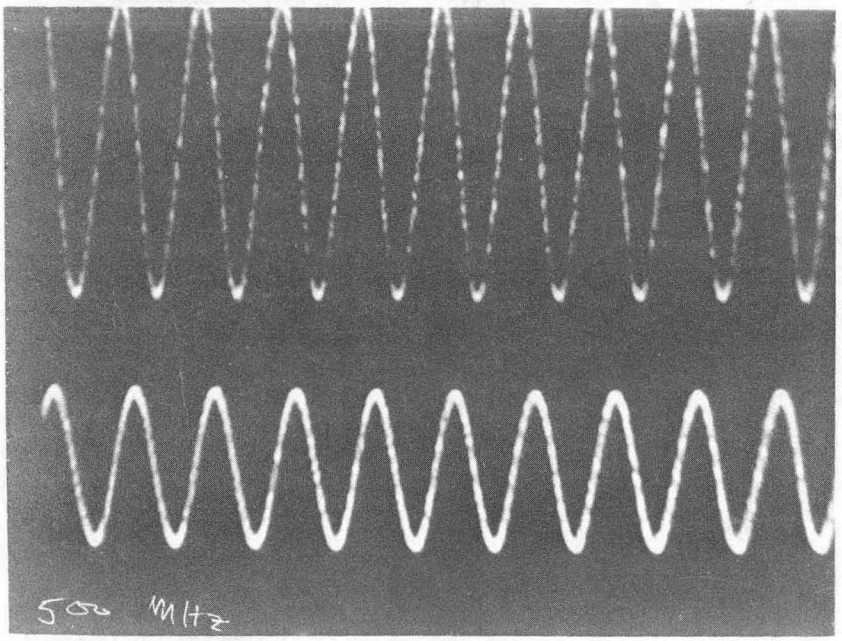

XBB 763-2687

Fig. III-4. R.f. signal display, 150 MHz and 500 MHz. Upper traces--signal in, lower traces--pickup coil.

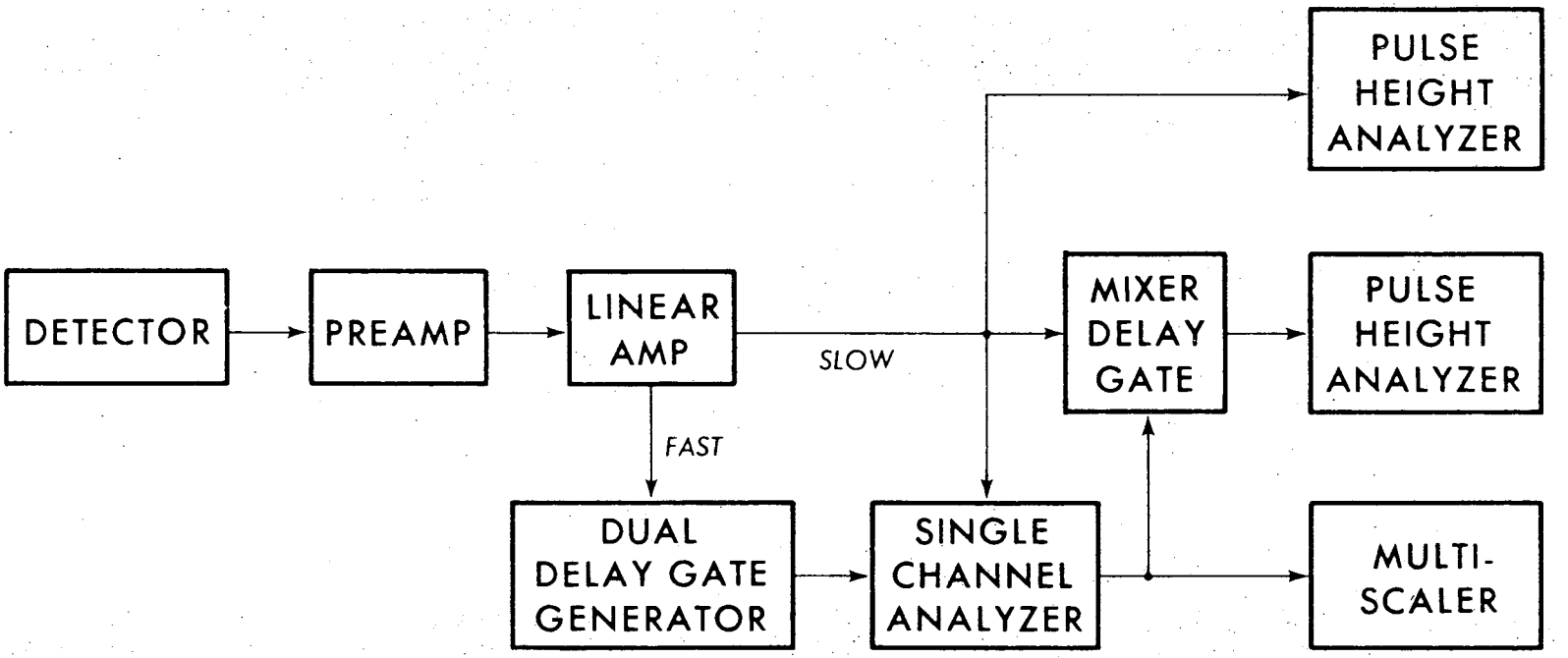

XBL 763-2508

Fig. III-5. Electronics--schematic.

G. Sample Preparation

The advances made in sample preparation during the course of these experiments have made significant contributions to the resolution in the spectra. The usual methods for making NMR/ON sources have been to make very thin foils (about 1μ) by successive rolling and annealing stages after either evaporating the radioactive trace impurity on the surface, reducing and diffusing under H_2,[78,79] by direct or back-scattering implantation following a nuclear reaction,[81] or production in situ in an accelerator. Some early work in single crystals of Fe seemed to indicate that such narrower lines could be obtained in a single crystal.[73] Unsuccessful attempts were made at the metallography lab in MMRD and by several commercial suppliers of metal single crystals to grow crystals of the dilute alloys.

One of the significant contributions to the line broadening must be the variation in the demagnetizing field throughout the sample. In a thin foil it is impossible to keep the wrinkles down even to the same magnitude as the thickness of the foil. Thus nuclei in a part of the foil oriented at some angle out of the plane of the polarizing field may well see a different net field than nuclei in other parts. A 1% CoFe spectrum from a foil prepared in this way is shown in Fig. III-6. Only a broadening to high field is noticeable. Kieser et al.[82] noticed a narrowing of the linewidth in the ^{60}CoFe resonance as they reduced the external polarizing field, and attributed this to a reduction in the overall variation in the demagnetizing field. It is likely that some of the improvement in the linewidths in the single crystal resonances was also due to the surface polishing the samples received.

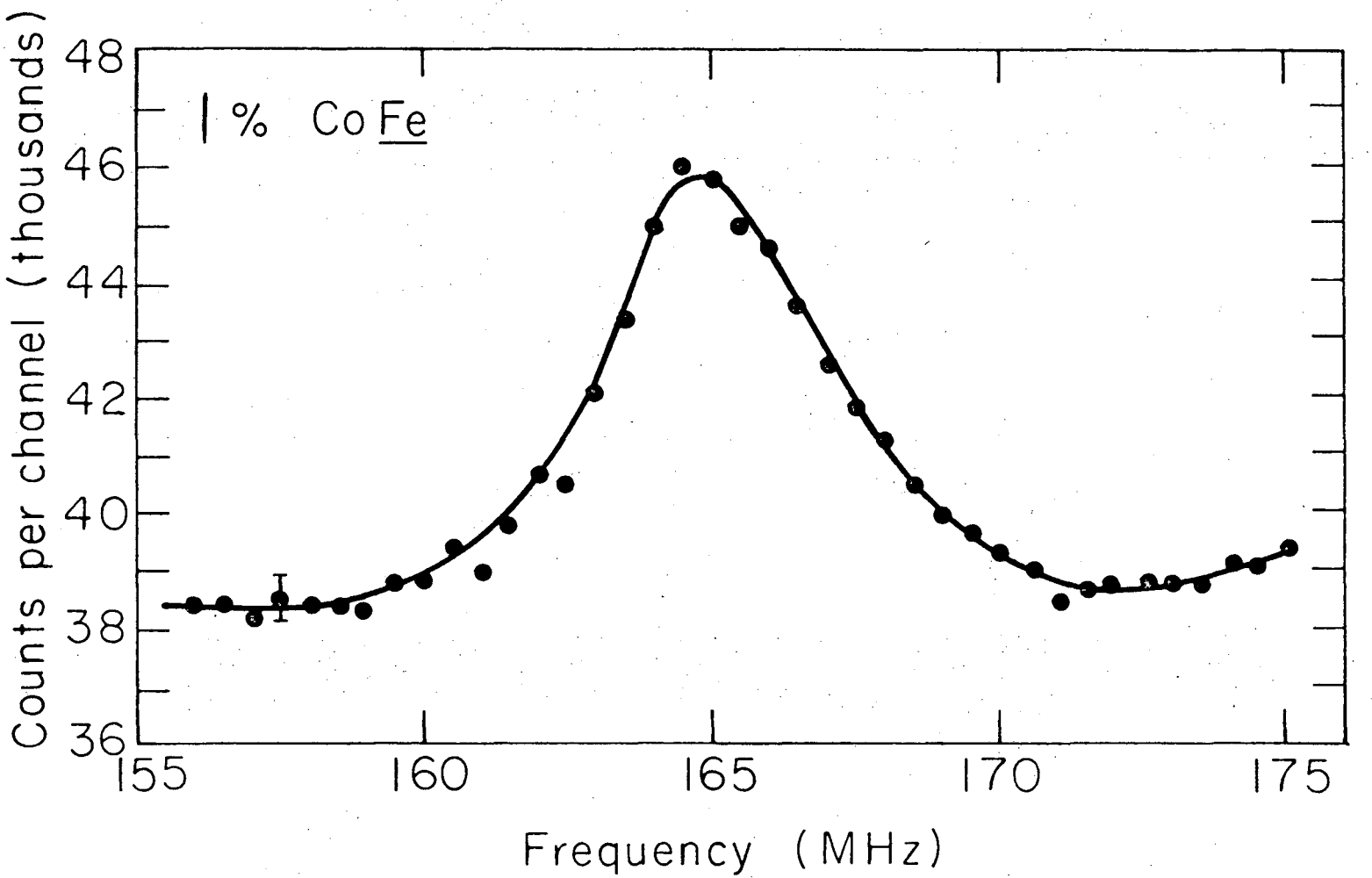

NBL 762-2280

Fig. III-6. Early 1% CoFe foil spectrum.

The following method evolved for the production of the samples used in this study. It was felt that if surface irregularities and damage could be reduced significantly below the rf skin depth (a few microns), the nuclei would have a better chance of seeing a more homogeneous field. Variations on the method might well be useful for other NMR/ON experiments where improved linewidth or resolution is desired.

(i) High purity starting materials--99.95+% Co^{83} and Ni^{84} and 99.999% Fe--[84] were cut and weighed before melting in an Argon arc furnace.[84] The ingot was turned and remelted several times to assure homogeneity, then weighed again after cooling. In all samples used, losses were less than a mg in sample weighing 1 to 2 grams.

(ii) The ingots were annealed under vacuum or 1/2 atm of H_2 at 1100°C for approximately 1 week.

(iii) The beads were soldered to rods and a machined down to a cylindrical diameter of 1/4 in.

(iv) Approximately 0.020 in. thick discs were cut on an Isomet[85] slow speed diamond saw which produces discs with parallel faces and fairly good surfaces.

(v) The discs were mounted in "Koldmount"[86] to facilitate handling and mechanically polished through a series of abrasive papers: 240 grit, 0, 00, 000 and 0000 turning through 90° each time to ensure removal of the damage layer from the previous paper.

(vi) The samples were than polished with 6μ diamond paste with kerosene as a lubricant on a canvas covered lapping wheel, turning at several hundred rpm, for several hours. The same treatment was repeated using 1μ polish.

(vii) Finally, mirror smooth surfaces were obtained by polishing for periods of up to 1 hr in a Syntron[87] vibrating polisher using a 0.05μ Al_2O_3 and lapping oil slurry. This gives a smooth, flat, pit free surface. Electropolishing does not improve the surfaces for these purposes as it results in a wavy or pitted surface unless very carefully controlled.

(viii) $^{60}CoCl_2$ solution,[88] after clean-up on an ion exchange column was dried on a leached planchette and the residual HCl was removed by repeated washing and drying cycles. The activity was electroplated onto a small platinum coil from a very small amount of NH_4OH at pH 10, with a bias of 2.2 volts. Using the hot Pt coil as an anode and again using ammonia as the electrolyte, approximately 10 to 50μCi of ^{60}Co was plated onto each sample which was then sealed in a quartz tube under 1/2 atm of H_2 and the activity diffused into the sample

The diffusion must be carried out below the α-γ phase transition, as the smooth surface can be destroyed by microcrystal reorientation in going back and forth between the phases. This poses no problem for the CoFe alloys as the α-γ transition temperature is relatively constant with alloy composition.[89] For the NiFe alloys, however, the transition temperature drops rapidly with increasing Ni concentration and the diffusions had to be carried out for long periods at low temperatures. Using the diffusion coefficient for ^{60}Co in Fe[90,91] it was calculated and found practicable to diffuse the CoFe samples for ~15 min at 850°C, while up to 30 days at 700°C was used for the 3.645 NiFe samples. After the diffusion step, the samples were annealed

for 24 hr at 600°C followed by a slow (50°C/hr) cooling to room temperature.

It might be pointed out that the enthalpy of solution of hydrogen in iron is positive and thus it is extremely insoluble.[92] Some of the samples were prepared using H_2 in the annealing stages and some were in vacuum (10^{-7} Torr). No effect on the spectra was observed.

(ix) The samples were attached to the cold fin of the CMN pill using Pb-Sn or Bi-Cd eutectic solder. The surfaces were protected throughout with a layer of laquer or by being laquered face down to a small quartz plate, which could in fact be left in place during the experiment.

IV. RESULTS AND DISCUSSION

The NMR/ON spectra for 0.56, 0.97, 1.93, 2.94 and 3.77% CoFe and 1.11, 2.09 and 3.64% NiFe are shown in Figs. IV-2 through IV-9. The fits and satellite assignments for the lower concentration alloys are given in Tables IV-2 through IV-6 adjacent to the spectra. Details of the methods used to obtain the data and various considerations in the assignments will be discussed below.

A. Statistical Distributions

For a random distribution of impurities in the alloy, the probability that n of N sites in a particular shell will be occupied by the impurity can be expressed as

$$P(n|N) = \frac{N!}{n!(N-n)!} c^n (1-c)^{N-n} \qquad \text{(IV-1)}$$

where c is the impurity concentration, Fig. IV-1. In the analysis which follows, only the first four shells will be considered as the 5^{th} and 6^{th} shells in the bcc alloy have only 8 and 6 sites respectively and they are expected to cause only small perturbations in the moment and hyperfine field distributions, evident only as an increased broadening. The notation used for representing the configurations is as follows.

The number of impurity substituents in each of the four shells surrounding an impurity site will be given in the form $(n_1 n_2 n_3 n_4)$. For example, (0110) means a Co site with no impurity in the first neighbor shell (N1), one impurity in the second shell (of 6 sites), one in the third and none in the fourth, etc. The probability of a given configuration of the first four shells is the product of the individual $P(n|N)$. Table IV-1 gives the calculated intensity ratios, normalized

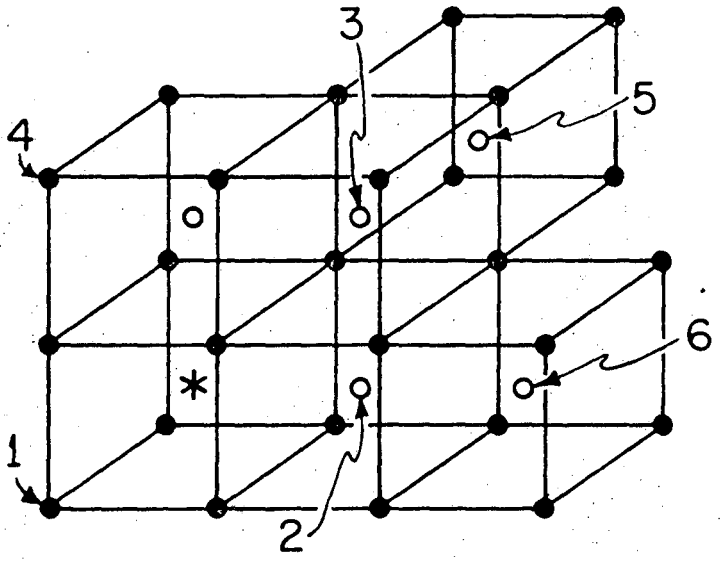

Shell no.	No. sites	Distance/a_0
1	8	$\sqrt{3}/2$
2	6	1
3	12	$\sqrt{2}$
4	24	$\sqrt{11}/2$
5	8	$\sqrt{3}$
6	6	2

Probability of n sites out of N being occupied

$$p(n|N) = \frac{N!}{n!(N-n)!} \quad c^n (1-c)^{N-n}$$

c = impurity concentration

XBL 762-2283

Fig. IV-1. Body-centered cubic lattice sites.

Table IV-1. Normalized statistical intensity ratios.

Configuration	0.56%	0.97%	1.11%	1.93%	2.09%
(0000)	1.000	1.000	1.000	1.000	1.000
(0001)	0.135	0.235	0.269	0.472	0.512
(0002)		0.026	0.035	0.107	0.126
(0003)				0.015	0.020
(0010)	0.068	0.118	0.135	0.236	0.256
(0011)		0.028	0.036	0.112	0.131
(0012)				0.025	0.032
(0020)				0.026	0.030
(0021)				0.012	0.015
(0100)	0.034	0.059	0.067	0.118	0.128
(0101)		0.014	0.018	0.056	0.065
(0102)				0.013	0.016
(0110)				0.028	0.033
(0111)				0.013	0.017
(1000)	0.045	0.078	0.090	0.157	0.171
(1001)		0.018	0.024	0.074	0.087
(1002)				0.017	0.021
(1010)			0.012	0.037	0.044
(1011)				0.018	0.022
(1100)				0.019	0.022
(1101)					0.011
(2000)				0.011	0.013

to the (0000) probability for concentration up to ~2%. Only those configurations having a normalized statistical probability greater than 0.010 are given. For the more concentrated samples, many more configurations contribute (e.g., 54 configurations for the 3.77% alloy with the above criterion) and meaningful assignments are not possible. In these cases the fits were done simply to provide an estimate of the total integrated areas, especially in the main satellite region.

Raw data from the multiscaler output were corrected for the background anisotropy change due to the gradual warming of the sample during the resonance sweep. The fits were performed using deconvolution programs SUNDER and GAMET on the Lawrence Berkeley Laboratory CDC 7600 computer. Allowed parameters are FWHM, centroid position, areas, background slope, etc. Various parameters can be fixed. For example, widths within a group of peaks could be required to be a certain value, or merely required to have all the same width; areas or area ratios may be fixed, splittings can be specified; peak shapes can be specified--whether Gaussian, Lorentzian or a mixture; etc. Most of these sophisticated capabilities were not used and the routines were given considerable freedom to fit the data. Gaussian lineshapes were used throughout as the inhomogeneous broadening factors are expected to be essentially random in nature. Some fits were made using Lorentzian lineshapes, or Gaussian-broadened Lorentzians, but the matches to the experimental data were not satisfactory, as would be expected since the inhomogeneous broadening is by far the largest contribution to the linewidth.

B. Spectra and Considerations in the Fits

Initial fits of the most dilute (0.56% and 0.97%) CoFe spectra allowed a shoulder on the high frequency side of the main peak, a doublet in the main satellite and a peak to low frequency. The only restriction placed on the fit was that all the widths be the same. There is no a priori reason for the widths to be the same, and, in fact, dipolar broadening is expected to affect the nearest neighbors significantly, but it is a reasonable starting point. The peak that was fitted to the high frequency shoulder of the main line had intensity which was very close in almost every case to the predicted intensity for an N4 substituent. This is in agreement with most of the assignments from spin-echo spectra for the Fe sites; beyond the first fits this peak area ratio was fixed to the statistical probability to speed convergence and reduce the number of free fit parameters. The main satellite was consistently fitted, with full freedom to a doublet whose intensity ratios were very close to 2:1 as would be expected for N3:N2, but with slightly more intensity compared to the main, unshifted line, than predicted. The peak to low frequency was, therefore, assumed to be due to an N1 substituent. Improvement in the fits was obtained if this low field satellite was allowed to broaden, independently of the others, and the program consistently converged on widths about 1.5 times as great as the main line.

The spectra, area ratios for the peaks, their frequency shifts, and widths are given in Figs. IV-2 to IV-9 and adjacent Tables IV-2 to IV-6, except for the more concentrated samples where the multitude of configurations contributing intensity make assignments meaningless.

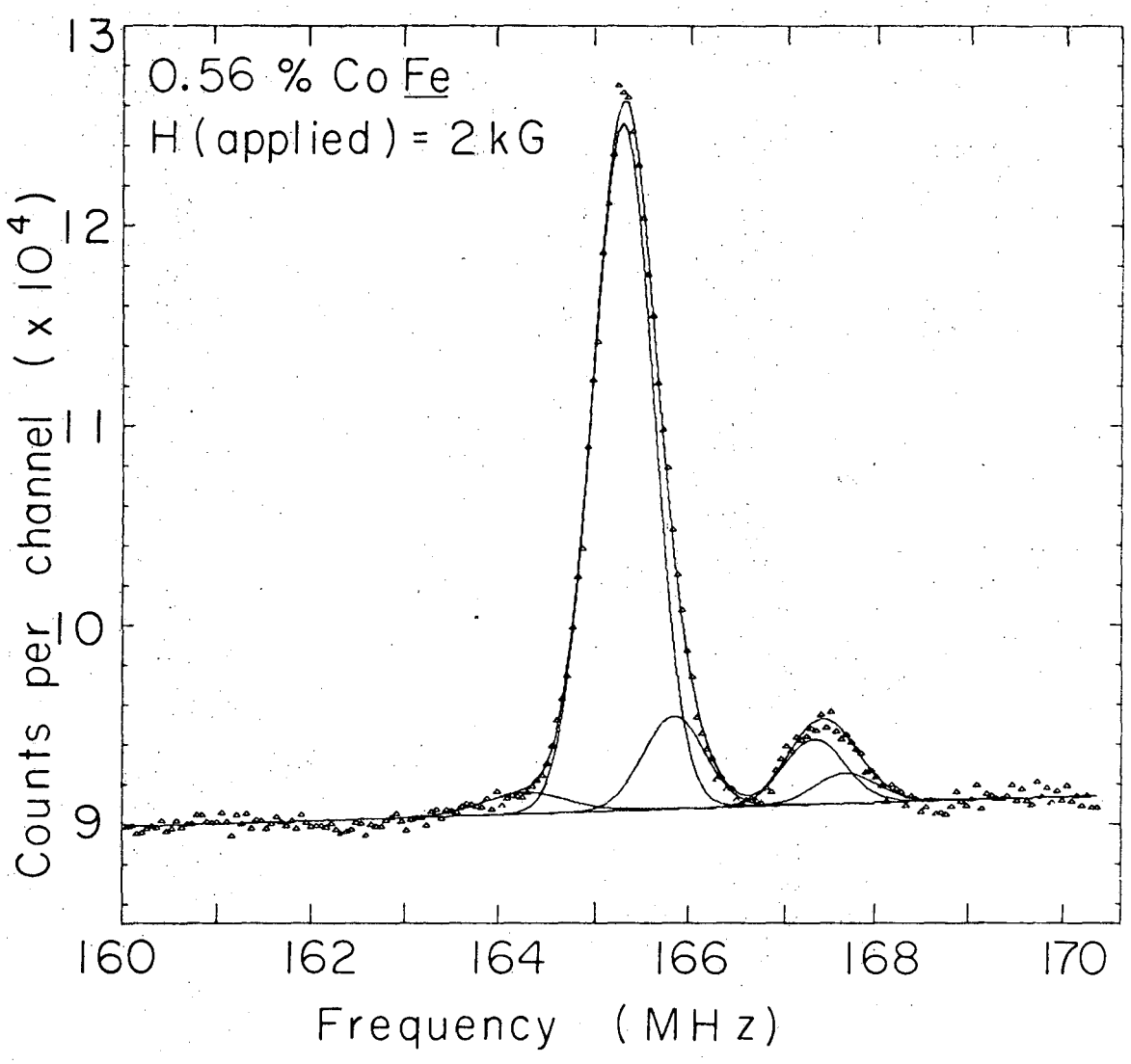

Fig. IV-2.

Table IV-2. Fits for 0.5640 CoFe.

Peak	(0000)	(0001)	(0002)	(0010)	(0100)	(1000)
Frequency (MHz)	165.28	165.82	--	167.31	167.63	164.24
Shift (MHz)	0.00	0.54	--	2.03	2.35	-1.04
		±0.02	--	±0.08	±0.19	±0.08
Intensity Ratio	1.0	0.135*	--	0.095	0.044	0.041
FWHM (MHz)	0.752	0.752	--	0.752	0.752	0.999†

*Fixed.

†Allowed to vary, independent of the others.

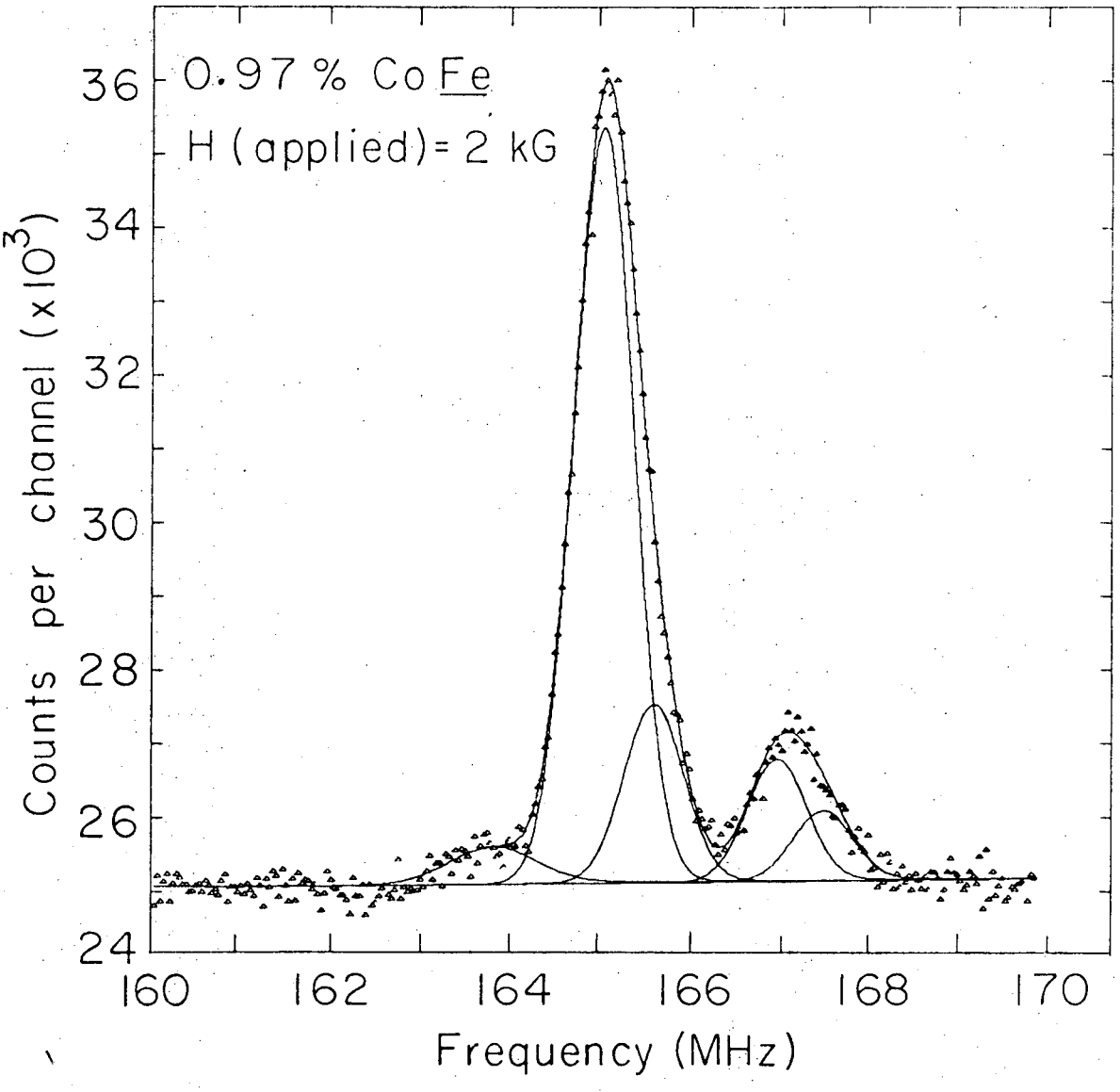

NBL 762 2294

Fig. IV-3.

Table IV-3. Fits for 0.97 CoFe.

Peak	(0000)	(0001)	(0002)	(0010)	(0100)	(1000)
Frequency (MHz)	165.05	165.62	--	166.99	167.50	163.83
Shift (MHz)	0.0	0.57	--	1.94	2.45	-1.22
		±0.01		±0.03	±0.05	±0.06
Intensity Ratio	1.0	0.235*	--	0.160	0.092	0.072
FWHM (MHz)	0.779	0.779	--	0.779	0.779	1.14**

*Fixed.

**Alloyed to vary, independent of the others.

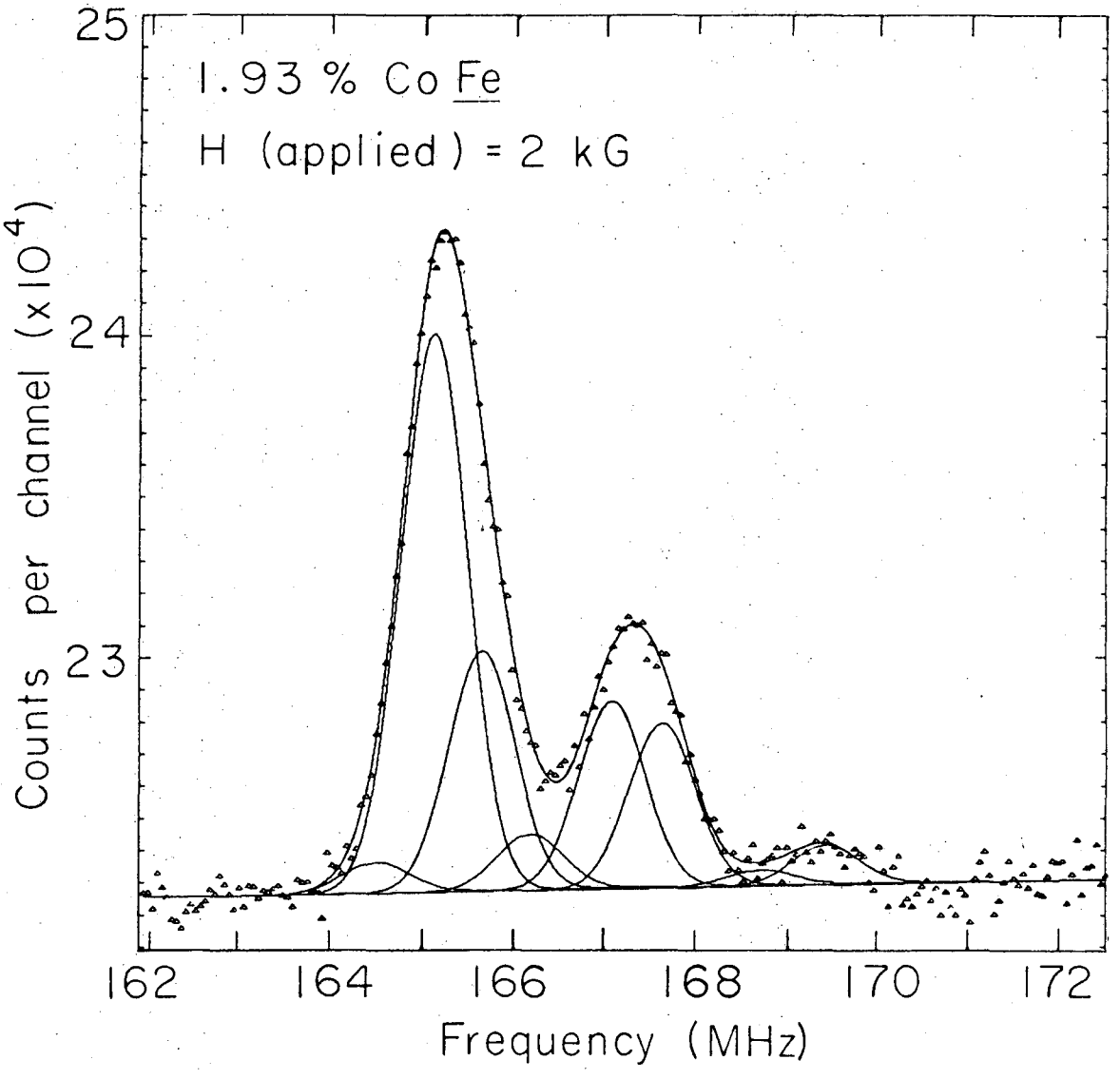

NBL 762-2292

Fig. IV-4.

Table IV-4. Fits for 1.93% CoFe.

Peak	(0000)	(0001)	(0002)	(0010)	(0100)	(1000)
Frequency (MHz)	165.13	165.67	166.20	167.12	167.68	164.48*
Shift (MHz)	0.0	0.54	1.07	1.99	2.55	-0.65*
		±0.02	±0.05	±0.04	±0.05	
Intensity ratio	1.0	0.430†	0.100†	0.336	0.294	0.055*
FWHM (MHz)	0.867	0.867	0.867	0.867	0.867	0.867

*Considered unreliable--not used in average of shifts or rest of analysis. See text.

†Fixed.

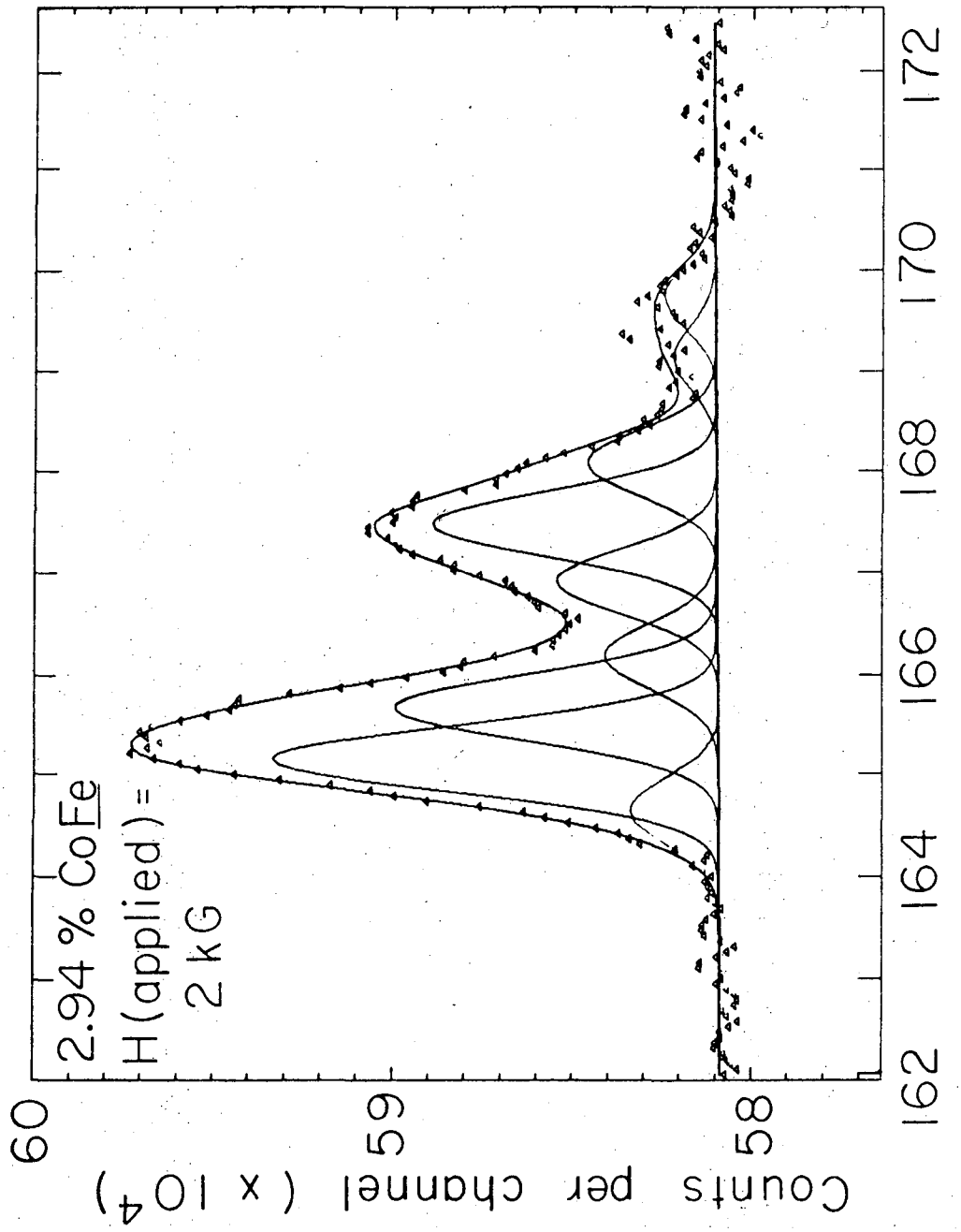

Fig. IV-5.

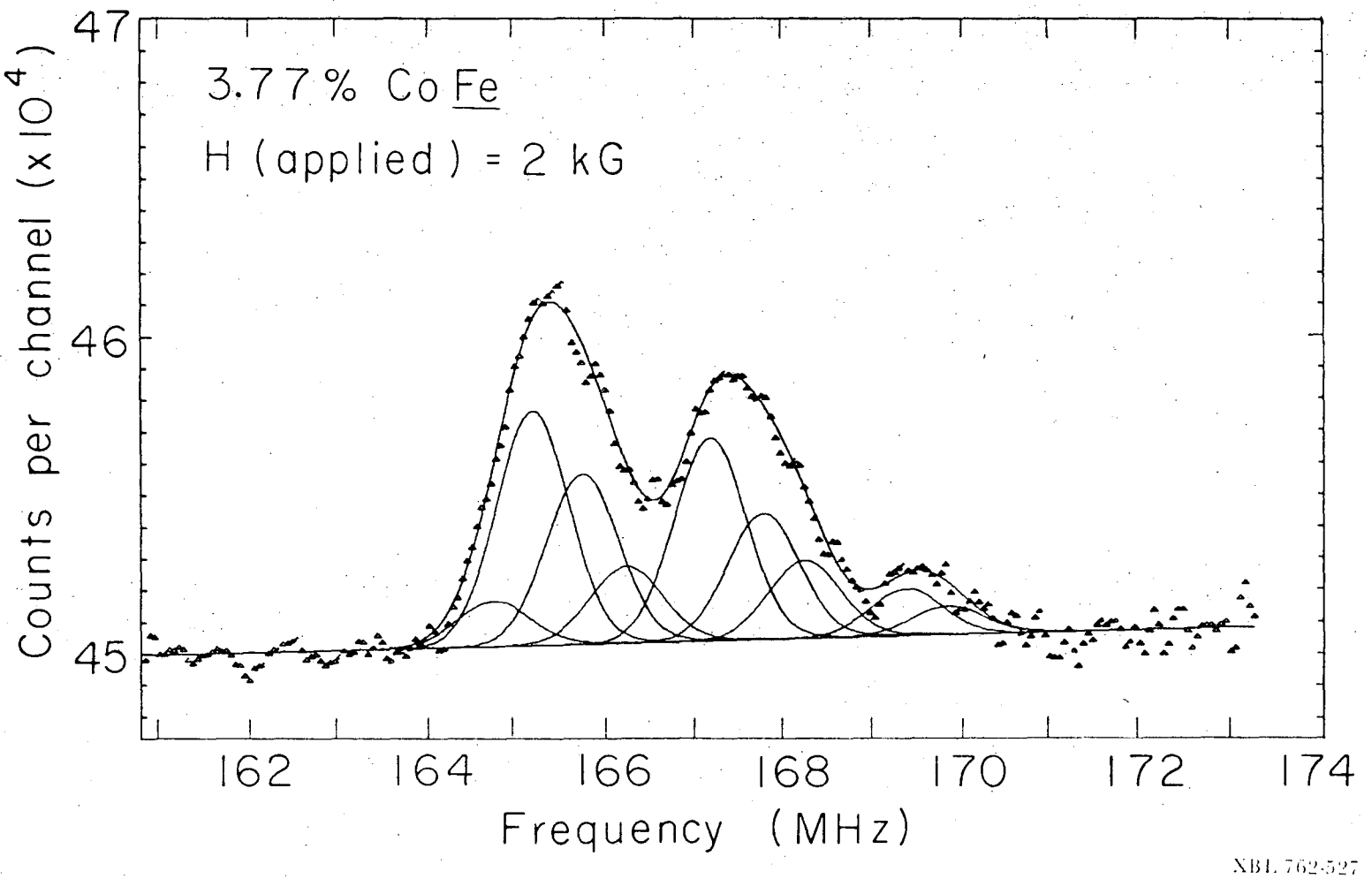
3.77% Co Fe
H (applied) = 2 kG
Counts per channel (x 10^4)
47
46
45
162
164
166
168
170
172
174
Frequency (MHz)
NBL 762-527

Fig. IV-6.

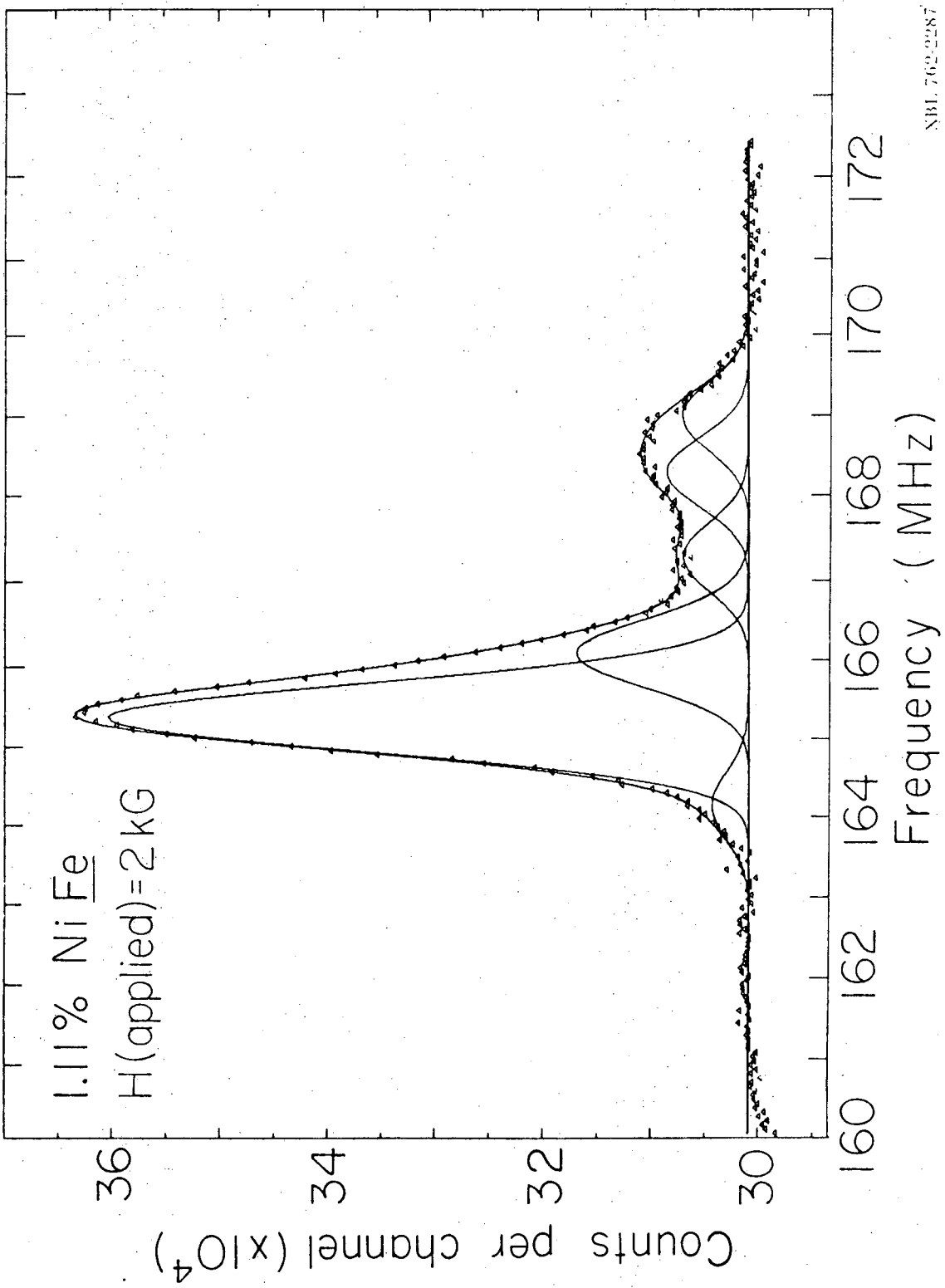

NBL 762-2287

Fig. IV-7.

Table IV-5. Fits for 1.11% NiFe.

Peak	(0000)	(0001)	(0002)	(0010)	(0100)	(1000)
Frequency (MHz)	165.24	166.03	167.23	168.28	168.97	167.23
Shift (MHz)	0.0	0.79	1.99*	3.04	3.73	1.99*
		±0.01	±0.13	±0.08	±0.10	±0.13
Intensity ratio	1.0	0.269†	0.035*	0.129	0.104	0.068*
FWHM (MHz)	0.995	0.995	0.995	0.995	0.995	0.995

*(1000) and (0002) in approximately the same position, and intensities sum to peak shown.

†Fixed.

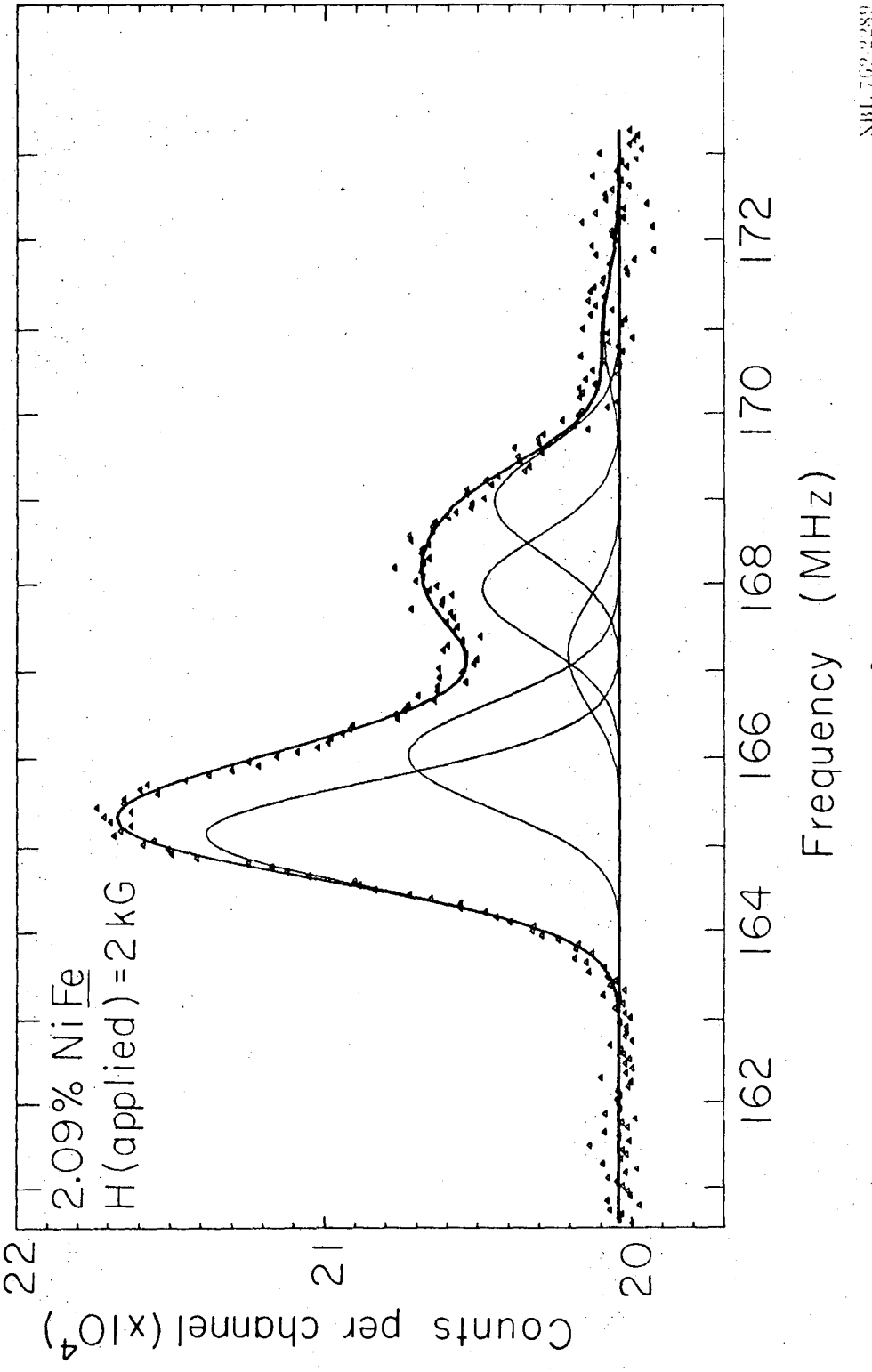

NBL 762-2289

Fig. IV-8.

Table IV-6. Fits for 2.09% NiFe.

Peak	(0000)	(0001)	(0002)	(0010)	(0100)	(1000)
Frequency (MHz)	165.03	165.94	167.11	167.86	168.87	--
Shift (MHz)	0.0	0.91	2.08	2.83	3.84	--
		±0.03	±0.06	±0.06	±0.06	
Intensity ratio	1.0	0.512†	0.126†	0.331	0.302	--
FWHM (MHz)	1.44	1.44	1.44	1.44	1.44	--

†Fixed.

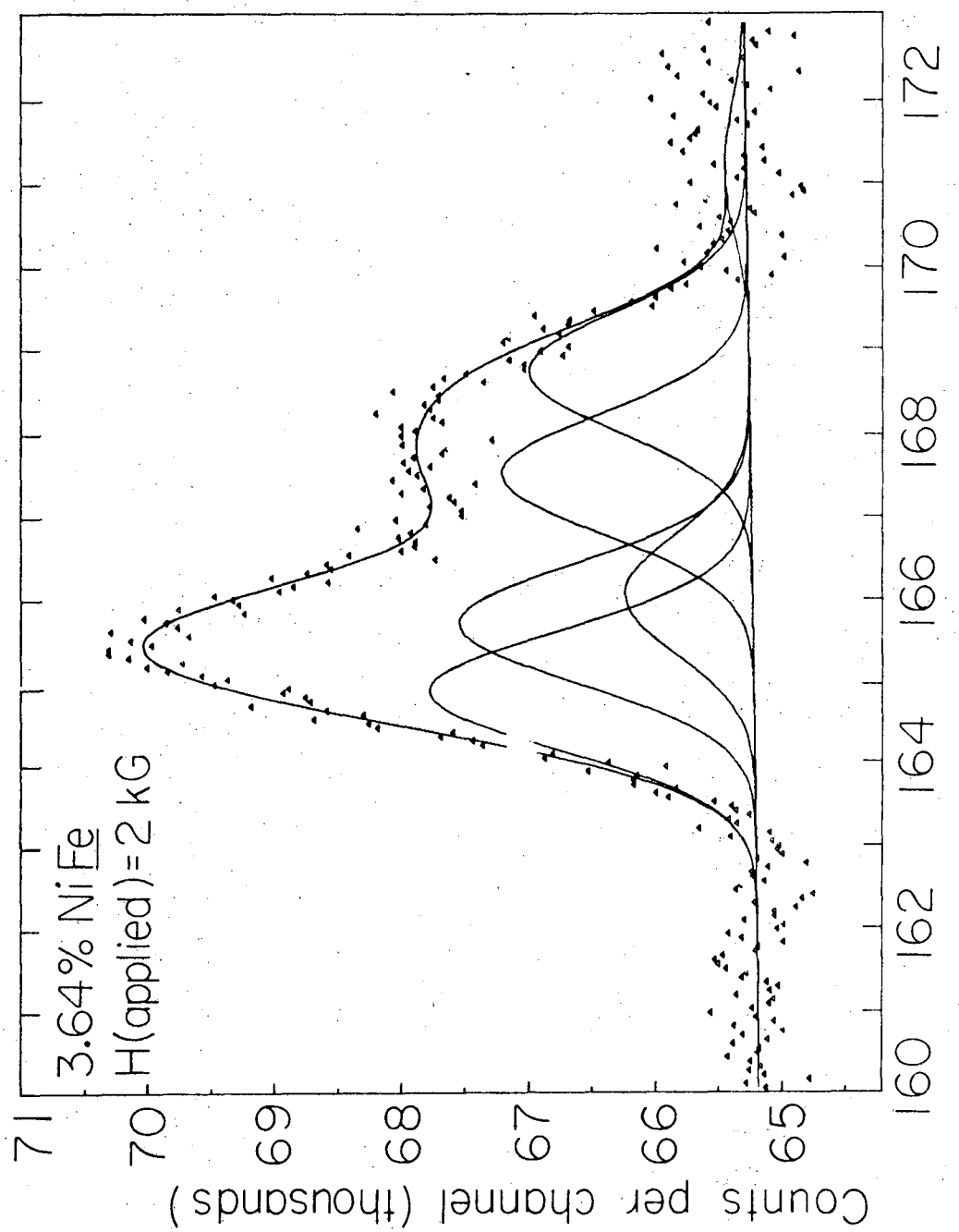

XBL 762-2291

Fig. IV-9.

Fig. IV-10 shows the experimental and theoretical main satellite intensities for the more dilute CoFe samples, considering the most significant configurations.

As noted above, if the assignment of (0010) and (0100) to the main satellite is correct, there is more intensity here than predicted for a statistical distribution. One another possibility is to interchange the (0100) and (1000) assignments. This would require the (0100) to be the origin of the broad low frequency peak and such a rapid oscillation in the field shifts is not really expected. The dipolar broadening expected for the N1 shell supports the assignment of the low frequency peak to N1 since it is consistently wider than the rest of the low concentration alloys and in fact is not statistically significant at all in the more concentrated samples, presumably being broadened into the baseline or lost in the statistics. Putting (1000), (0100) and (0010) all in the satellite and having N5 or N6 shifts negative is also possible, but the shift of the low frequency peak is too great for this to be a viable alternative.

There is insufficient intensity in the main satellite to account for all of the (1000), (0100) and (0010) configurations, especially in light of several points to be discussed below. For example, the 0.56% sample has a normalized intensity of 0.139 in the satellite while at least 0.156 would be required if (1000), (0100), (1000) and (0011) are all shifted into this region.

It may be recalled that much of the spin-echo and Mössbauer work on the Fe alloys showed far too little satellite intensity compared to the later studies, and that this had led to much of the confusion

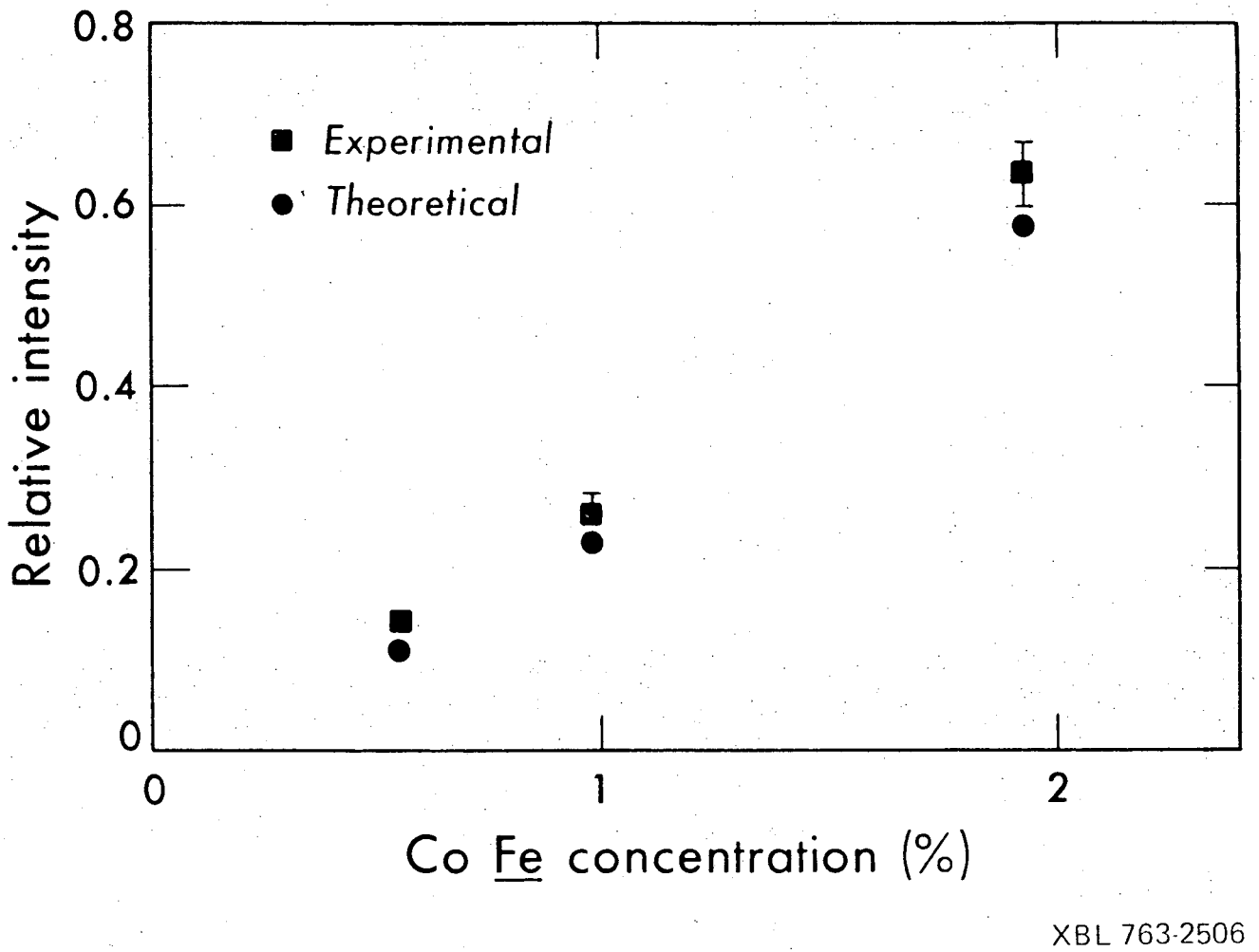

Fig. IV-10. Experimental and calculated main satellite intersites for CoFe spectra.

in the assignments for the Fe sites. It is not too difficult to explain away attenuated intensities, but more intensity than expected must be rationalized.

Several aspects of the NMR/ON technique must be considered. First, of course, is the fact that the amount of anisotropy destoryed is not necessarily a linear function of the number of nuclei involved at a particular frequency. The resonance saturates at a level below full isotropy and this would lead to a reduction in the amplitude of large peaks compared to small peaks. This is only of real significance if the amount of anisotropy destroyed is a considerable fraction of that available. In all but the lowest concentration CoFe, sample the maximum resonant destruction is less than about a 10% effect so this aspect can probably be neglected.

Configurations such as (0101) and (0011) will produce intensity in the satellite but will be very insignificant for low concentrations as seen in Table IV-1.

The concentrations of the alloys are well known and assumed homogeneous. However, the addition of the ^{60}Co and whatever carriers may not have been removed in the cleanup procedure may contribute to the impurity concentration. A sample prepared in the same manner as the alloys, but consisting only of 99.999% Fe plus the ^{60}Co plated onto it showed no satellites in the resonance and only a very slight high field shoulder which is probably due to relaxation effects or possibly a quadrupole term in the hyperfine Hamiltonian. This latter point will be discussed below. Incorrect concentration, however, can probably be eliminated as a source of the intensity.

There is, however, a chemical effect involved in the alloy preparation. From a chemical point of view, Co and Fe (and Ni) are different species and in the production of the alloys it is reasonable that the Co either would rather have nearest neighbor Co's or it would rather not. Near 50%, CoFe forms a CsCl superlattice,[93] with alternating Co and Fe sites, suggesting that the latter is the case. This was pointed out by Wertheim[26] who prepared samples by quenching rapidly to prevent ordering, and has been observed by Khoi et al.[21] in some spin-echo studies of three component systems. Burch et al.[94] noted that impurities in Fe_3Si alloys always tend to go into one of the two possible Fe sites which is presumably energetically favorable. The long annealing stages and diffusion at moderate temperatures might well permit such ordering in the alloys in this series of experiments.

Thus if the nearest neighbor to an observed ^{60}Co is more likely to be an Fe than in a fully random alloy, the N2 and N3 sites might be slightly enriched, accounting for the observed increased intensity. In addition, the weak low field satellite assigned as due to N1 in the CoFe spectra is slightly weaker than would obtain from a statistical distribution, but the counting statistics make detailed analysis of this point a bit unreasonable.

It is clear, then, in view of all these effects, that the low field satellite is a broadened peak due to an N1 substituent in the CoFe alloys.

A low frequency peak was allowed in the fits for all the spectra, including the high concentration CoFe and the NiFe samples where no

significant intensity was noted. Figure IV-7 for the 1.11% NiFe sample shows only a very small low frequency satellite which is not really separable from the main line. There is, however, considerable intensity between the main line and the main (0100) and (0010) satellite which is attributable to the (0002) plus (1000) in NiFe. The change in sign of the hyperfine field shift for the N1 substituent is not unreasonable since the shifts are highly sensitive to the radial distances and the hyperfine field shift "node" seems to occur between the N1 and N2 positions in CoFe.

The NiFe spectra, consistent with assigning a positive N1 frequency shift, show total shifted intensities (0.759 for the 2.09% and 1.84 for the 3.64%) which can only be accounted for by including the (1000) and (1001) and similar configurations with high frequency shifts (totaling 0.84 and 2.05 predicted intensities, respectively, for the most significant configurations). In addition, the deconvolution routine, with the signal to noise ratio available in these runs, repeatedly abnegated the existence of a low frequency satellite in the high concentration NiFe runs. Figure IV-11 shows the total experimental main satellite intensities for some NiFe spectra and the predicted intensities for the major configurations with shifts at these frequencies.

The higher concentration CoFe spectra clearly show weak, further shifted satellites with intensities and shifts which correspond roughly to those expected for configurations such as (0110), (0111), (0020), and various other "higher order" weak configurations. These are in qualitative agreement with the additivity assumptions.

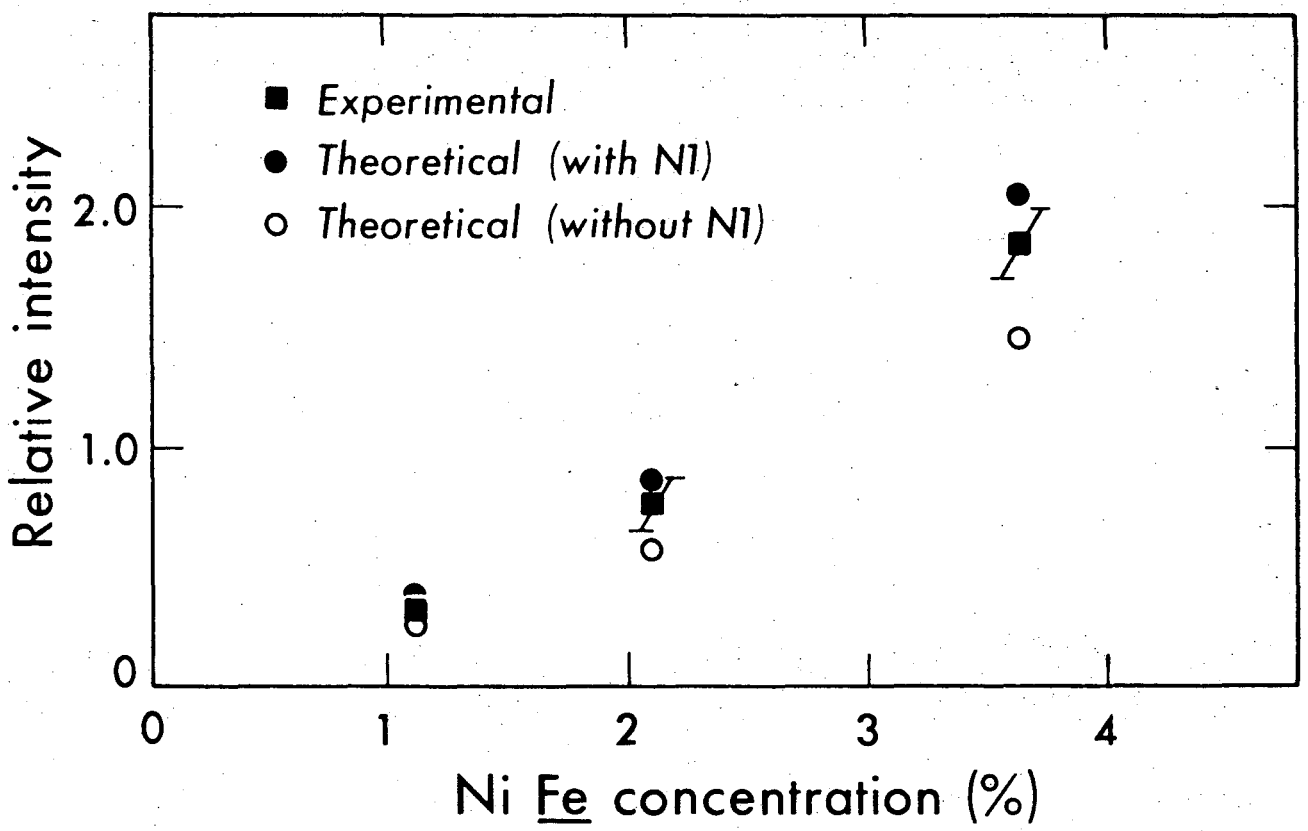

XBL 763-2505

Fig. IV-11. Experimental and calculated main satellite intensities for NiFe spectra.

For concentration much above 1% of course, the assignments pretty much fall apart due to the increased probability that other configurations enter into consideration. The only attempt to take this into account was the adjustment of the fixed (0001) and (0002) intensities in the CoFe spectra by considering that a (1001) configuration would give amplitude in an essentially unshifted position and contribute to the main line.

In the higher concentration spectra, the broadening expected due to the contribution of many weaker configurations, and the worsening signal to noise ratio precludes the assignment of peaks to particular configurations and the Gaussians shown in the spectra were fitted mainly to provide information regarding the total integrated intensity. Thus it is only for the more dilute alloys where a clear picture of the relative intensities, and reasonably unambiguous assignments can be made, that the hyperfine field shifts due to neighboring impurities have been calculated. The shifts are given in Table IV-7 and are plotted as a function of position in Fig. IV-12.

C. Quadrupole Effects and Fast Passage Experiments

Now, to return to the consideration of quadrupole effects, Callaghan et al.[95-97] have shown that the existence of a nuclear quadrupole interaction, which requires a finite elastic field gradient at the nucleus can be detected by NMR/ON in cubic materials. The field gradients might arise from the arrangement of the neighboring ions or from the electrons on the particular ion itself, if there remains some unquenched orbital angular momentum. This is generally assumed to be quenched by the cubic crystal fields although for high

Table IV-7. ^{60}Co hyperfine field shifts.

Substituent	MHz	H (kG)
CoFe		
(0001)	0.56±0.03	-0.98±0.05
(0010)	1.98±0.04	-3.41±0.07
(0100)	2.48±0.10	-4.28±0.17
(1000)	-1.08±0.13	+1.86±0.22
NiFe		
(0001)	0.85±0.08	-1.49±0.14
(0010)	2.94±0.15	-5.14±0.26
(0100)	3.79±0.08	-6.63±0.14
(1000)	1.99±0.13	-3.48±0.23

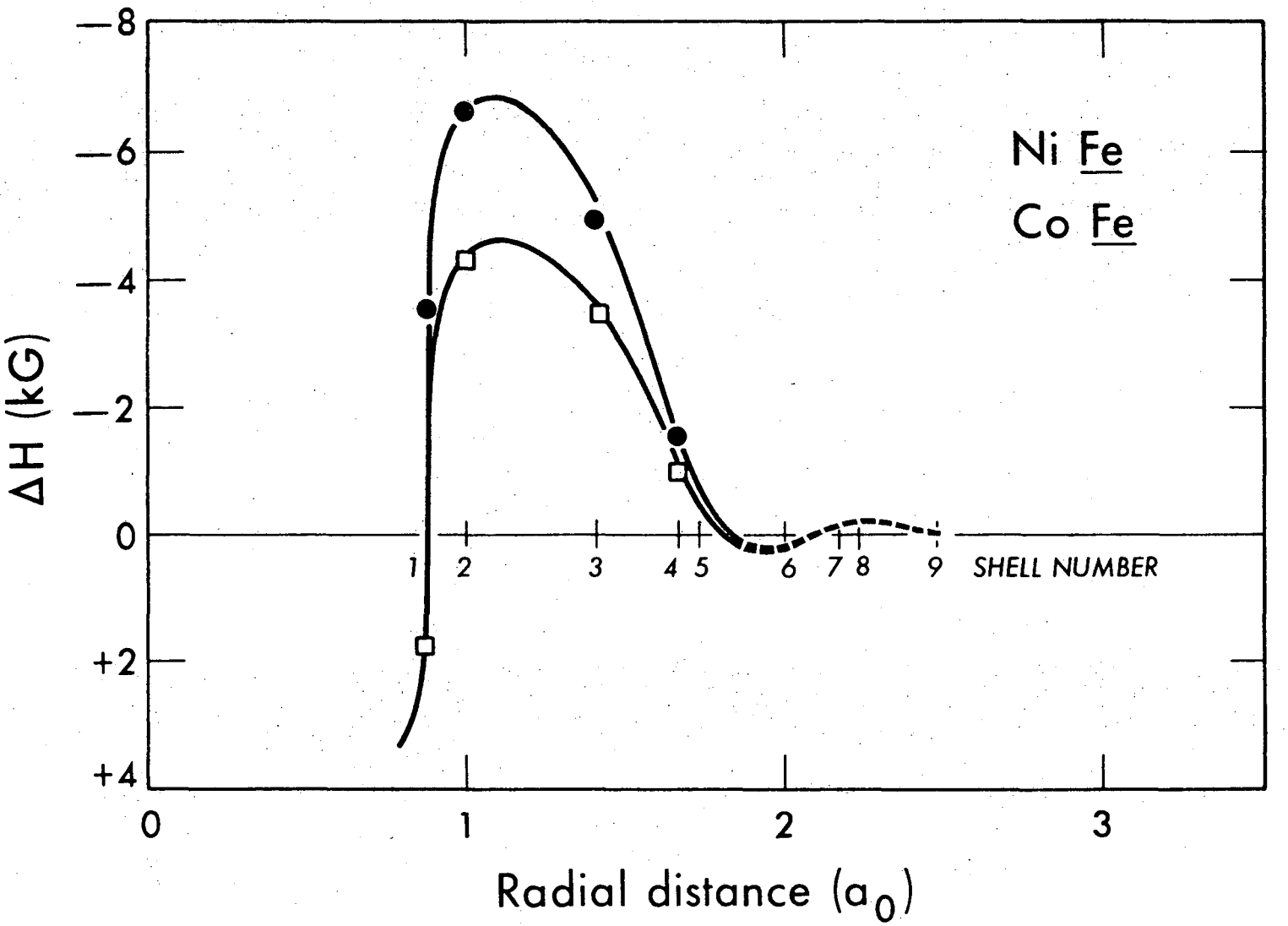

Fig. IV-12. ^{60}Co hyperfine field shifts in CoFe and NiFe alloys.

XBL 763-2509

Z impurities, such as Au or Ir, orbital contributions to the magnetic hyperfine interaction have been reported.[98,100] The proximity of vacancies, lattice defects, and magnetostriction effects could break the cubic symmetry and give rise to nonzero field gradients.

To observe the effect in the NMR spectrum in the usual methods as used in this study of the alloys, the quadrupole term in the Hamiltonian would have to be quite large, perhaps 10-20%, with respect to the inhomogeneously broadened linewidth and to the FM width, otherwise transitions between the unequally split levels would still be possible. However, if a single fast passage sweep is made through the resonance, with no frequency modulation, a cyclic inversion of populations can occur. This results in a sweep direction dependence of the response, since the time evolution of the orientation parameters after passing through resonance is highly sensitive to the initial perturbed sublevel population. Callaghan et al.[101] have shown the results for such single passage runs in ^{60}CoFe foils with residual FM less than 100 Hz bandwidth. There was a considerable sweep direction dependence. The experiment was repeated in the apparatus at Berkeley with virtually identical results, using a oscillator with stability of about 1 part in 10^8. The Oxford group also did the fast passage run with an FM of 20 kHz and observed no sweep direction dependence, from which it can be concluded that the quadrupole term must be smaller than this. For ^{198}AuFe, very large sweep direction dependences could be observed, from which a P = 0.21 MHz could be explicitly calculated.[99]

We have done the fast passage experiment on a 1% CoFe sample (Fig. IV-13) and again see results almost identical to those of the "pure" sample and conclude that the quadrupole term, while present is much less than the linewidths, and is not significantly altered by the high impurity concentrations. It can, therefore, be neglected in the consideration of the alloy spectra obtained using slow sweeps and several hundred kHz FM. The results also suggest that the origin of the quadrupole term is probably due to some unquenched orbital angular momentum on the Co site since the high impurity concentration would quite drastically change any effects arising from crystal fields themselves, defects, etc, and this is not observed.

In a pure polycrystalline sample of Fe (Fig. IV-14) a small high field shoulder is observed, which may have a contribution from the quadrupole term, but is probably due more to the finite spin-lattice relaxation time compared to the sweep rate. The resolution in the alloy spectra is such that these effects would only lead to a slight additional broadening.

Future studies of alloy hyperfine field distributions should, however, take account of the quadrupole term in the Hamiltonian if definitive conclusions are to be drawn.

D. Comparison with Model Parameters

In terms of the Stearns model parameters discussed in Chapter I, the hyperfine field shifts at the impurity sites can be compared to those at the Fe sites as follows, where, for CoFe:

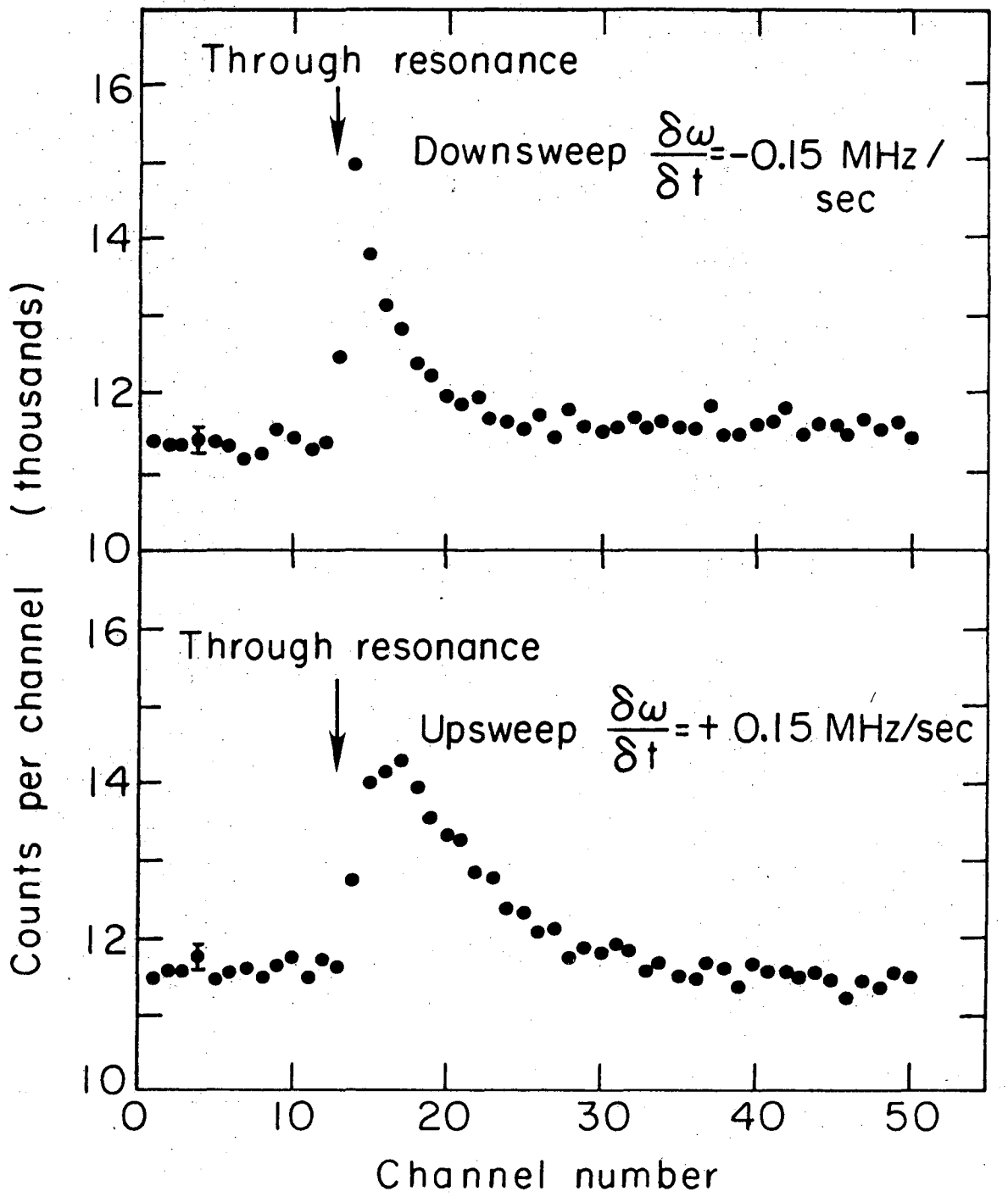

XBL 762-2279

Fig. IV-13.

Adiabatic fast passage resonance sweeps.

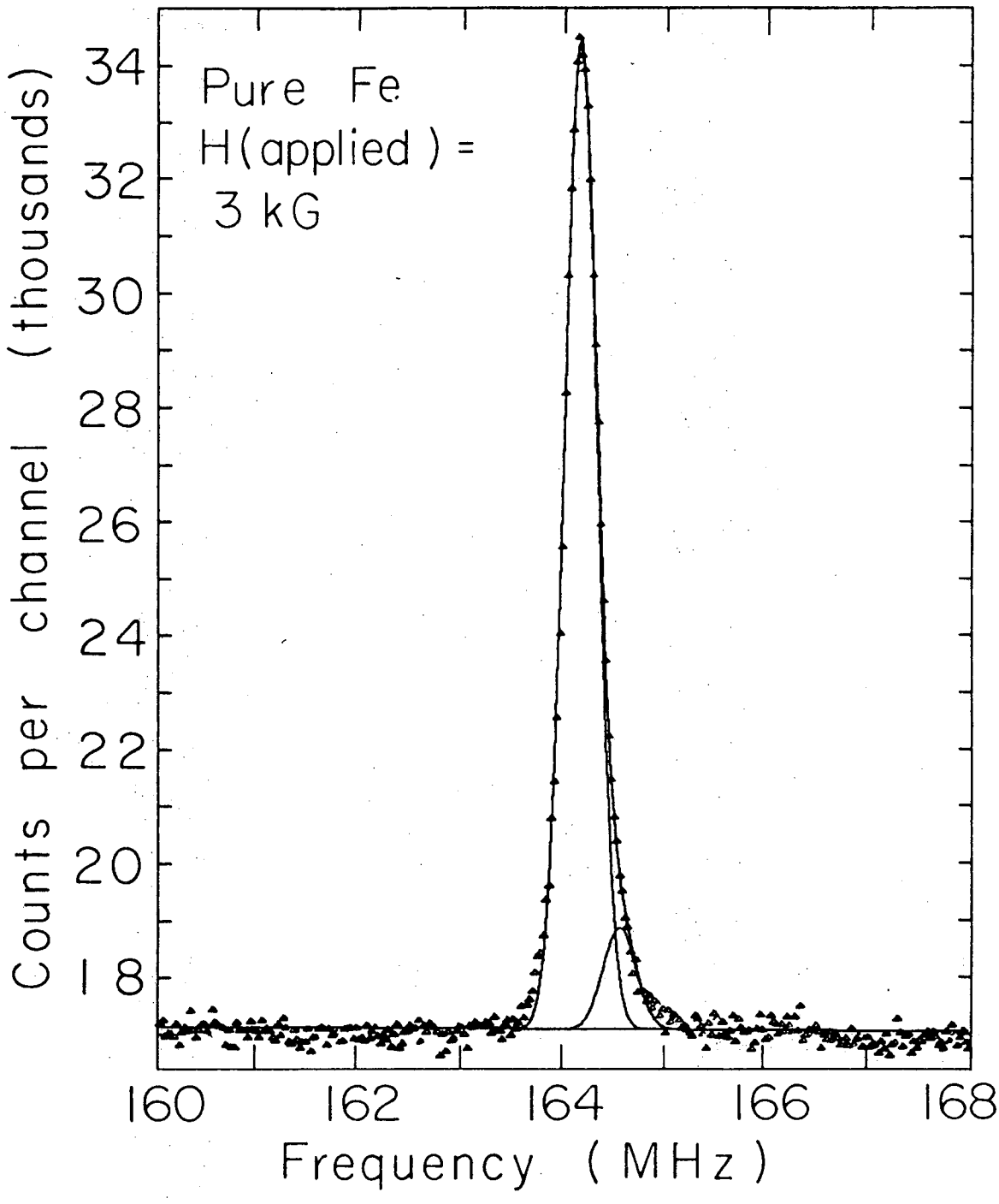

XBL 762-2285

Fig. IV-14.

$\Delta H_n \equiv$ the s CEP due to the n^{th} shell in pure Fe

$\Delta_n \equiv$ increase in the Fe moment in the n^{th} shell surrounding a Co atom

$\delta_n \equiv$ increase in the Co moment in the n^{th} shell surrounding a Co atom

$\Delta H_{Co}^{Nn}(Co) \equiv$ shift in Co hyperfine field in the n^{th} shell surrounding a Co atom

$\Delta H_{Fe}^{Nn}(Co) \equiv$ shift in Fe hyperfine field in the n^{th} shell surrounding a Co atom

Then

$$\Delta H_{Co}^{Nn}(Co) = (H_M + \Delta H_n)(\delta_n - \Delta_n) + \Delta H_{Fe}^{Nn}(Co) \qquad \text{(IV-2)}$$

From Stearns' Paper	This Work
$\Delta H_{Fe}^{N1}(Co) = -4.6$ kG	$\Delta H_{Co}^{N1}(Co) = +1.9$ kG
$\Delta H_{Fe}^{N2}(Co) = -6.5$	$\Delta H_{Co}^{N2}(Co) = -4.3$
$\Delta H_{Fe}^{N3}(Co) = -4.3$	$\Delta H_{Co}^{N3}(Co) = -3.4$
$\Delta H_{Fe}^{N4}(Co) = -1.9$	$\Delta H_{Co}^{N4}(Co) = -1.0$

The assignments of Stauss,[20] to admittedly rather poor spin echo spectra were (correcting the sign) 4.0, -3.6, -3.6 and -0.6 kG for the first four shells. In reasonable agreement with the present work. Aside from the N1 shift, Co has a slightly smaller hyperfine field shift than the Fe sites, indicating $\Delta_n > \delta_n$ which is reasonable, since the electrons are more localized on the Co and the Co moment is already nearly saturated. For NiFe:

$\alpha_n \equiv$ increase in Fe moment in the n^{th} shell surrounding a Ni atom

$\Delta_n \equiv$ increase in Fe moment in the n^{th} shell surrounding a Co atom

$\varepsilon_n \equiv$ increase in Co moment in the n^{th} shell surrounding a Ni atom

$\beta_n \equiv$ increase in Ni moment in the n^{th} shell surrounding a Co atom

Then, summing the contributions as before:

$$\Delta H_{Co}^{Nn}(Ni) = H_M(\varepsilon_n - \alpha_n) + H_n(\beta_n - \Delta_n) + \Delta H_{Fe}^{Nn}(Ni) \qquad \text{(IV-3)}$$

From Stearn's Paper	This Work
$\Delta H_{Fe}^{N1}(Ni) = -1.4$ kG	$\Delta H_{Co}^{N1}(Ni) = -3.55$ kG
$\Delta H_{Fe}^{N2}(Ni) = -7.7$	$\Delta H_{Co}^{N2}(Ni) = -6.6$
$\Delta H_{Fe}^{N3}(Ni) = -6.7$	$\Delta H_{Co}^{N3}(Ni) = -5.1$
$\Delta H_{Fe}^{N4}(Ni) = -2.8$	$\Delta H_{Co}^{N4}(Ni) = -1.5$

Again the shifts are generally smaller than for the Fe sites indicating $\alpha_n > \varepsilon_n$ and in keeping with same trend $\Delta_n > \beta_n$. The further the solute is to the right of Fe, the greater its moment perturbation. The positive hyperfine field shifts at the N1 sites in CoFe are consistent with the oscillatory CEP shifts which are very sensitive to the radial distance from the impurity. A reduction in the transferred hyperfine field is expected since the Co sees an N1 substituent with a smaller moment than if it were surrounded only by Fe's. In the NiFe alloys, this is presumably offset by a larger change

in the local moment on the Co site itself.

Quantitative estimates for the moment perturbation parameters are not yet possible as there is no means of separating the various contributions to H_M. Further studies with fcc Co and Ni as hosts might provide additional information regarding the various parameters, but there are technical problems involved in doing NMR/ON in these hosts which might preclude the acquisition of useful data without extreme difficulty.

V. CONCLUSIONS

Hyperfine field distributions at impurities in domains in dilute CoFe and NiFe alloys have been measured by NMR on oriented nuclei with good resolution, providing detailed information on hyperfine field shifts due to impurity neighbors. Although the spectra are comparable in resolution to the best spin-echo data, the originally hoped for high resolution was never quite achieved, and in fact it may not be possible to improve on it due to broadening from more distant shells. There is evidence to indicate some degree of ordering in the dilute alloys and a non-statistical distribution of the impurities. Quadrupole interactions in these alloys are insignificant with respect to the magnetic hyperfine interaction in terms of the resolution obtained in this work.

The spectra are consistent with a model in which the shifts are primarily caused by moment perturbations in neighboring shells surrounding an impurity, with RKKY-like spin density oscillations affecting the conduction electron and core polarization contributions to the hyperfine fields. Generally, Ni causes greater shifts than Co substituents neighboring a Co, although in neither case are the shifts as great as at the Fe sites. This is consistent with a reduced number of itinerant electrons in going across the 3d transition series and with the moment perturbations arising via the itinerant d's.

ACKNOWLEDGEMENTS

At this point, I would like to acknowledge the assistance, support and friendship of the many of my colleagues who have contributed in so many ways to my research and to my time spent in Berkeley in general.

Professor David A. Shirley directed this research, and I would like to thank him for his guidance and his patience. His physical insight and extensive knowledge were most helpful in clarifying my understanding of many aspects of this work.

I have benefitted greatly from my association with many of the visitors who spent various periods visiting our hyperfine interactions group. Professor Gene Westenbarger introduced me to various low temperature methods and Professor Günter Kaindl and Dr. Eberhard Mahnke spend considerable time with me in the early stages explaining the fundamental aspects and experimental "black magic" of low temperature research. I would especially like to thank Professor Ken Krane, with whom some of the early work on the dilute alloys was performed, for his assistance, particularly with the initial data analysis. Many helpful and informative discussions were held with Professor Charles Johnson and Professor Eckart Matthias and I wish to thank them for their help and interest.

Professor Joe Budnick has shown interest in this work and provided moral support and I would like to acknowledge several interesting conversations with Dr. Mary Beth Stearns and especially to thank her for suggesting the application of the model parameters to the impurity spectra.

My fellow graduate students have been a constant source of help, information, and frequently recreation and comic relief over the past 5 years. I would especially like to thank Dr. Art Soinski, Dr. Fred Bacon, Dr. Dan Salomon, Dr. T. S. Chou, Dr. Gary Schwartz, Sefik Süzer, Bernice Mills, Steve Kowalczyk, Rich Martin, Read McFeely and Gus Apai for their friendship and for the many hours spent with them in conversation and the pursuit of various interests, scientific and otherwise.

The support staff at the Lawrence Berkeley Laboratory will be missed also. Wini Heppler provided invaluable assistance with the chemical work and has been a very kind friend. Gerda Bolz and Betty James also oversaw the radiochemistry and watched out for my health and welfare. Ed Voronin built and helped design some of the apparatus and Lee Johnson was of great assistance in the metallurgical and metallographical aspects of the sample preparations.

Finally, I would like to thank my wife, Ursula, for her support and encouragement throughout, for putting up with the weird work schedule so often required in the low temperature experiments, for sharing so many of the joys and disappointments of my work, and for our life together.

This work was done under the auspices of the U. S. Energy Research and Development Administration. The financial assistance of the Department of Colleges and Universities Affairs of the Province of Manitoba, Canada, is also acknowledged. Any conclusions or opinions expressed in this report represent solely those of the author and not necessarily those of the Lawrence Berkeley Laboratory nor the U. S. Energy Research and Development Administration.

APPENDIX: SPIN-LATTICE RELAXATION TIMES

In a related part of this study, the longitudinal (spin-lattice) relaxation times of the ^{60}Co nuclei were measured in some of the alloys.

Assuming that spin-lattice relaxation occurs via a contact interaction with the conduction electrons, of the form

$$A\,\tilde{I}\cdot\tilde{S} = AS_zI_z + \frac{1}{2}A(S_+I_- + S_-I_+) \qquad \text{(A-1)}$$

Bacon et al.[102] showed that the transition probabilities between adjacent $|m\rangle$ states could be given by expressions in which the downward transition probability consisted of two terms, a temperature dependent part which is equal to the upward probability and a temperature independent, spin dependent part. At very low temperatures a temperature independent relaxation time T_μ was described as the low temperature limit of T_1', a relaxation time measured by fitting the experimental curves to a single exponential decay.

The density of states at the Fermi surface is of course a factor in the transition probabilities since the magnetic relaxation mechanism allows transitions between adjacent $|m\rangle$ states by a spin-flip excitation in the conduction electrons. The electron must be scattered from a (filled) state below E_F to an empty, available state above E_F. In the high temperature case, the Korringa relation applies since the number of states available is proportional to the temperature. For low temperatures, where $h\nu > kT$, only electrons within $h\nu$ of the Fermi surface can undergo the transition and the transition probability becomes temperature independent. The nuclear spin dependence arises

since it is the $|m=I\rangle$ to $|m=I-1\rangle$ and $|m=1-I\rangle$ to $|m=-I\rangle$ transitions which are slowest and thus rate determining. Thus, T_μ is defined as

$$T_\mu = \lim_{T\to o} T_1' = \frac{kC}{h\nu I} = \frac{kC}{\mu H} \qquad \text{(A-2)}$$

where C is the high temperature Korringa constant. The full details of the theoretical aspects are developed by Bacon et al.[102]

Assuming a rigid band model, it might be expected that the addition of small amounts of Co, which has one more electron, to Fe, would shift the Fermi level out. In heat capacity measurements[103-105] there appears to be a sharp maximum in the transition metal Fermi level density of states curve at Fe. If the density of states (d.o.s.) curve at the Fermi level in Fe changes rapidly as the Fermi energy is shifted, then large changes in the relaxation time would be expected for small changes in Co concentration. If on the other hand, the d.o.s. curve is fairly flat in this region, which has indeed been indicated by most recent calculations[106,107] and by photoemission studies,[108] only small changes would be expected.

Measured T_1's for some 1, 2 and 4.4% CoFe alloy thin foils are shown in Fig. A-1.

The relaxation times were measured by applying rf at the resonant frequency and modulating over the peak of interest until the resonance is saturated. When the modulation is turned off, the nuclei relax back to an equilibrium Boltzmann distribution. The rf carrier signal is left on, thereby ensuring constant eddy-current heating and establishing a constant or very slowly changing lattice temperature. The count rate as a function of time after turning off the modulation

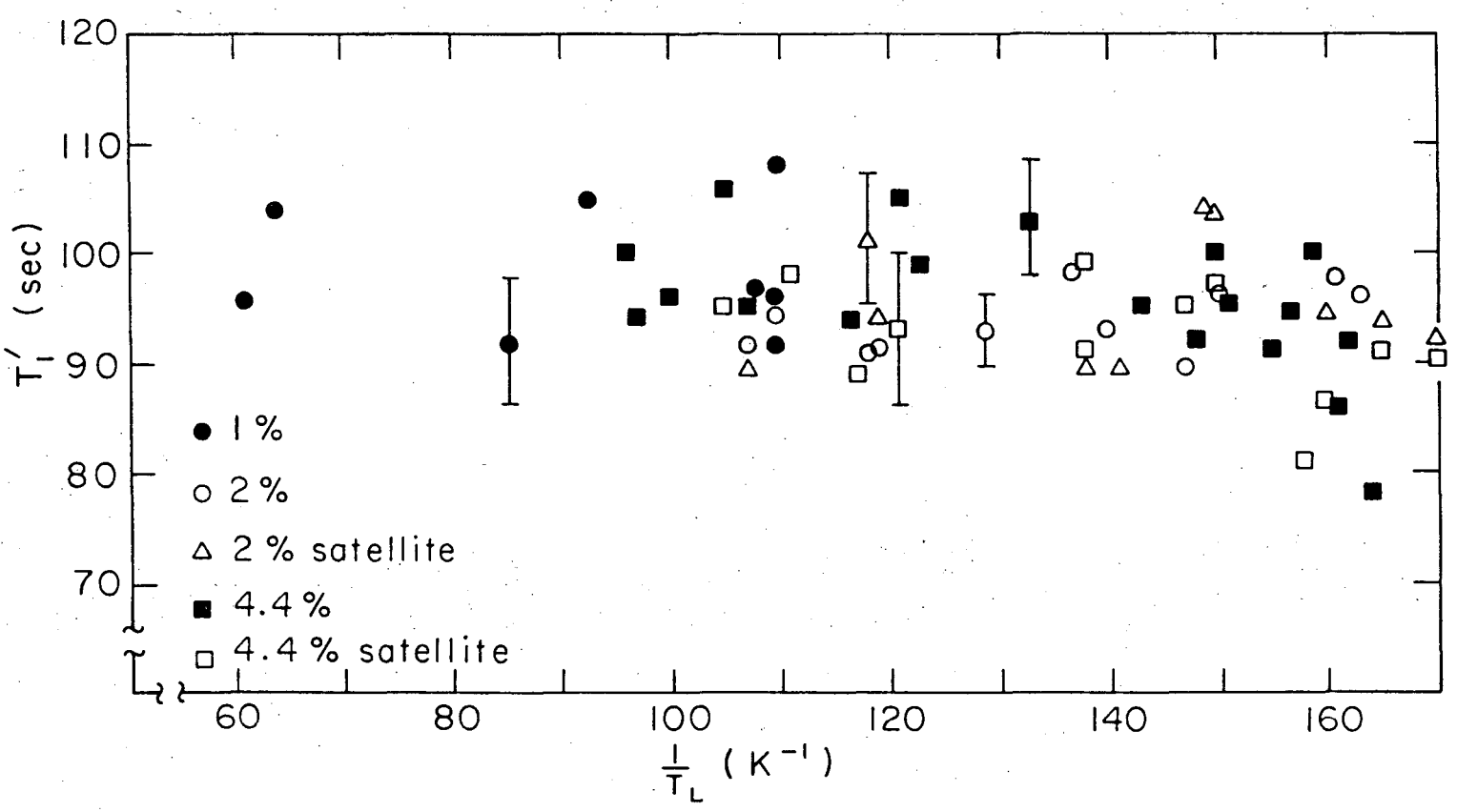

Fig. A-1. Spin-lattice relaxation times for some CoFe alloy foils.

was fitted to a single exponential with a sloping straight line background to allow for slight sample warmup during the run. The method has been fully described by Barclay.[78]

The effects of the different hyperfine fields and conduction electron d.o.s. for sites with impurity neighbors might be made apparent by saturating only the main peak in the spectrum and observing the relaxation and comparing the T_1's to those obtained by setting the rf on the main satellite, measuring the relaxation times of those nuclei having N2 or N3 Co neighbors. The relaxation times for the satellite line in the 2 and 4.4% alloys are also shown in Fig. A-1.

Unfortunately, the poor counting statistics and difficulties in measuring T_1's in this way lead to large uncertainties in the calculated relaxation times. No significant change can be noted as a function of concentration and the small effect due to the ~1% change in the hff at the satellites is not at all observable.

There is, however, an apparent maximum in the T_1' before reaching a saturation value due to the fact that the other decay constant (other than the slowest $h\nu I/kC$) are not that much faster than $1/T_1'$. This has been dealt with in a general theory by Wolfle and Götze[109,110] who also derive a temperature in dependent, spin dependent relaxation time.

REFERENCES

1. M. F. Collins and G. G. Low, Proc. Phys. Soc. 86, 535 (1965).
2. I. A. Campbel, Proc. Phys. Soc. 89, 71 (1966).
3. S. W. Lovesey, Proc. Phys. Soc. 89, 893 (1966).
4. I. A. Campbell and A. A. Gomès, Proc. Phys. Soc. 91, 319 (1967).
5. H. R. Child and J. W. Cable, Oak Ridge National Laboratory Report No. 74-107 (75-64), to be published in Phys. Rev. B.
6. R. C. LaForce, S. F. Ravitz and G. F. Day, Phys. Rev. Lett. 6, 226 (1961).
7. Y. Koi, A. Tsujimura, T. Hihara and Y. Kushida, J. Phys. Soc. Japan 16, 574 (1961).
8. R. L. Streever, L. H. Bennet, R. C. LaForce and G. F. Day, Phys. Rev. 128, 1632 (1962).
9. G. V. H. Wilson, Proc. Phys. Soc. 84, 689 (1964).
10. E. F. Mendis and L. W. Anderson, Phys. Rev. Lett. 19, 1434 (1967).
11. E. F. Mendis and L. W. Anderson, Phys. Stat. Sol. 41, 375 (1970).
12. E. F. Mendis, Ph. D. Thesis, University of Wisconsin, 1969.
13. E. F. Mendis, J. Phys. F: Metal Physics 4, L59 (1974).
14. J. Aslam and W. Weyhmann, Univ. of Minnesota Report COO-1569-71 (1971).
15. M. Rubinstein, G. H. Stauss, and M. B. Stearns, J. Appl. Phys. 37, 1334 (1966).
16. M. Rubinstein, Phys. Rev. 172, 277 (1968).
17. J. J. Murphy, J. I. Budnick and S. Skalski, J. Appl. Phys. 39, 1239 (1968).
18. J. I. Budnick, T. J. Burch, S. Skalski and K. Raj, Phys. Rev. Lett. 24, 511 (1970).

19. J. J. Murphy, T. J. Burch and J. I. Budnick in AIP Conference Proceedings #10, part 2, Magnetism and Magnetic Materials (1972), p. 1627.

20. G. H. Stauss, Phys. Rev. B4, 3106 (1971).

21. L. D. Khoi, P. Veillet and I. A. Campbell, J. Phys. F: Metal Physics 4, 2310 (1974).

22. C. E. Johnson, M. S. Ridout and T. E. Cranshaw, Proc. Phys. Soc. 81, 1079 (1963).

23. T. E. Cranshaw, C. E. Johnson and M. S. Ridout, Phys. Lett. 21, 481 (1966).

24. T. E. Cranshaw, J. Phys. F: Metal Physics 2, 615 (1972).

25. G. K. Wertheim, V. Jaccarino, J. H. Wernick and D. N. E. Buchanan, Phys. Rev. Lett. 12, 24 (1964).

26. G. K. Wertheim, Phys. Rev. B1, 1263 (1970).

27. G. K. Wertheim, D. N. E. Buchanan and J. H. Wernick, J. Appl. Phys. 42, 1602 (1971).

28. I. Vincze and I. A. Campbell, J. Phys. F: Metal Physics 3, 647 (1973).

29. W. E. Sauer and R. J. Reynick, J. Appl. Phys. 42, 1604 (1971).

30. M. B. Stearns, Phys. Rev. 147, 439 (1966).

31. A. C. Gossard and A. M. Portis, Phys. Rev. Lett. 3, 164 (1959).

32. A. M. Portis and A. C. Gossard, J. Appl. Phys. 31, 205S (1960).

33. A. M. Portis and J. Kanamori, J. Phys. Soc. Japan 17, 587 (1962).

34. J. Friedel, Nuovo Chim. (Suppl. 2) 7, 287 (1958).

35. E. Daniel and J. Friedel, J. Phys. Chem. Solids 24, 1601 (1963).

36. M. B. Stearns, Phys. Rev. 162, 496 (1967).

37. M. B. Stearns and J. F. Ullrich, Phys. Rev. B4, 3825 (1971).

38. G. A. Murray and W. Marshall, Proc. Phys. Soc. 86, 315 (1965).

39. M. A. Butler, Phys. Rev. B8, 5122 (1973).

40. M. B. Stearns, Phys. Rev. B4, 4081 (1971).

41. A. Blandin, in Magnetism, H. Suhl, ed. (Academic Press, 1973), Vol. V, p. 58.

42. A. Narath, ibid, p. 149.

43. M. B. Stearns, Phys. Rev. B9, 2311 (1974).

44. M. B. Stearns, to be published in Phys. Rev. B.

45. M. B. Stearns, private communication.

46. D. I. Bardos, J. Appl. Phys. 40, 1371 (1969).

47. P. Weiss and R. Forrer, Ann. Phys. 5, 153 (1926).

48. R. E. Watson and A. J. Freeman, J. Appl. Phys. 32, 118S (1961).

49. R. E. Watson and A. J. Freeman, Phys. Rev. 123, 2027 (1961).

50. W. Marshall and C. E. Johnson, J. de Phys. et Rad. 23, 783 (1962).

51. D. A. Shirley and G. A. Westenbarger, Phys. Rev. 138, A170 (1965).

52. D. A. Shirley, S. S. Rosenblum and E. Matthias, Phys. Rev. 170, 363 (1968).

53. M. B. Stearns, Phys. Rev. B4, 4069 (1971).

54. F. E. Simon, in Comptes Rendus du Congrès sur le Magnetisme, Strasbourg, (1939).

55. M. E. Rose, Phys. Rev. 75, 213 (1949).

56. C. J. Gorter, Physica 14, 504 (1948).

57. B. Bleany, Proc. Phys. Soc. A64, 315 (1951).

58. M. A. Grace, C. E. Johnson, N. Kurti, R. G. Scurlock and R. J. Taylor, in Conference de Physique de Basses Temperature, Paris (1955).

59. B. N. Samoilov, V. V. Sklyarevskii and E. P. Stepanov, Zh. Eksperim. Teor. Fiz. 36, 644 (1959) (Sov. Phys. JETP 9, 448 (1959))

60. R. J. Blin-Stoyle and M. A. Grace, Encyclopedia of Physics, S. Flügge, ed. (Springer Verlag, Berlin, 1957), Vol. 42.

61. J. M. Daniels, Oriented Nuclei (Academic Press, NY, 1965).

62. C. D. Jeffries, Dynamic Nuclear Orientation (Interscience, NY, 1963).

63. D. A. Shirley, Thermal Equilibrium Nuclear Orientation in Ann. Rev. Nuclear Sci. 16 (1966).

64. O. V. Lounasmaa, Experimental Principles and Methods Below 1K (Academic Press, London, 1974).

65. M. Ferentz and N. Rosenzweig, Table of F Coefficients, Argonne National Laboratory Report ANL-5324 (1955).

66. K. Siegbahn, ed., Alpha, Beta and Gamma Ray Spectroscopy (North-Holland, Amsterdam, 1965).

67. K. S. Krane, Tables of Coefficients for Analysis of Angular Distribution of Gamma Radiation from Oriented Nuclei, Los Alamos Scientific Laboratory Report No. LA-4677 (1971).

68. A. Rutledge, Finite Geometry Corrections to Gamma Ray Angular Correlations . . ., Atomic Energy of Canada Report No. CRP-851 (1959).

69. D. C. Camp and A. L. VanLehn, Nucl. Inst. and Meth 76, 192 (1969).

70. E. Matthias and R. J. Holliday, Phys. Rev. Lett. 17, 897 (1966).

71. J. E. Templeton and D. A. Shirley, Phys. Rev. Lett. 18, 240 (1967).

72. D. A. Shirley, in Colloque A.M.P.E.R.E. XV (North-Holland, Amsterdam, 1969).

73. D. A. Shirley, in Hyperfine Interactions and Nuclear Radiations, E. Matthias and D. A. Shirley, eds. (North-Holland, Amsterdam, 1968).

74. N. J. Stone, in Hyperfine Interactions in Excited Nuclei, G. Goldring and R. Kalish, eds. (Gordon and Breach, NY, 1971), Vol. 1, p. 237.

75. A. M. Portis and R. H. Lindquist, in Magnetism, G. T. Rado and H. Suhl, eds. (Academic Press, NY, 1965), Vol. IIA.

76. J. I. Budnick, in Colloque A.M.P.E.R.E. XV (North-Holland, Amsterdam, 1969).

77. E. Matthias, B. Olsen, D. A. Shirley, J. E. Templeton and R. M. Steffen, Phys. Rev. A4, 1626 (1971).

78. J. A. Barclay, Thesis, Lawrence Radiation Laboratory Report No. UCRL-18986, 1969 (unpublished).

79. W. D. Brewer, Thesis, Lawrence Radiation Laboratory Report No. UCRL-19533, 1969 (unpublished).

80. F. Bacon, Thesis, Lawrence Berkeley Laboratory Report No. LBL-1271, 1972 (unpublished).

81. D. Spanjaard, R. A. Fox, J. D. Marsh and N. J. Stone, in Hyperfine Interactions in Excited Nuclei, G. Goldring and R. Kalish, eds. (Gordon and Breach, NY, 1971), Vol. 1, p. 113.

82. R. Kieser, N. Kaplan and B. G. Turrell, Phys. Rev. B9, 2165 (1974).

83. Leico Industries, New York, NY.

84. Materials Research Corporation, Orangeburg, NY.

85. Beuhler, Ltd, Evanston, IL.

86. Vernon-Benshoff Co., Albany, NY.

87. F. M. C. Corporation, Homer City, PA.

88. New England Nuclear, Boston, MA.

89. M. Hansen, Constitution of Binary Alloys (McGraw-Hill, 1958).

90. J. Askill, Bibliography on Tracer Diffusion in Metals, Part 2, Tracer Diffusion in Pure Metals, Oak Ridge National Laboratory Report No. ORNL-3795 (1965).

91. P. W. James and G. M. Leak, Phil. Mag. 14, 701 (1966).

92. J. Völkl and G. Alefeld, Hydrogen Diffusion in Metals, in Diffusion in Solids: Recent Developments, A. S. Nowick and J. J. Burton, eds. (Academic Press, 1975).

93. J. E. Goldman and R. Smoluchowski, Phys. Rev. 75, 140 (1949).

94. T. J. Burch, T. Litrenta and J. I. Budnick, Phys. Rev. Lett. 33, 421 (1974).

95. P. T. Callaghan, P. D. Johnston and N. J. Stone in International Conference on Hyperfine Interaction Studies in Nuclear Reactions and Decay, Abstracts of the Contribute Papers, E. Karlsson and R. Wäppling, eds., Uppsala, 1974, p. 202.

96. P. T. Callaghan, P. D. Johnston, W. M. Lattimer and N. J. Stone, ibid, p. 250.

97. P. D. Johnston, R. A. Fox and N. J. Stone, J. Phys. C: Solid State Phys. 5, 2077 (1972).

98. R. A. Fox and N. J. Stone, Phys. Lett. A29, 341 (1969).

99. P. T. Callaghan, P. D. Johnston, W. M. Lattimer and N. J. Stone, to be published.

100. P. D. Johnston and N. J. Stone, J. Phys. C: Solid State Physics 5, L303 (1972).

101. P. T. Callaghan, P. D. Johnston and N. J. Stone, J. Phys. C: Solid State Phys. 7, 3161 (1974).

102. F. Bacon, J. Barclay, W. Brewer, D. A. Shirley and J. Templeton, Phys. Rev. B5, 2397 (1972).

103. C. H. Cheng, C. T. Wei and P. A. Beck, Phys. Rev. 120, 426 (1960).

104. F. Heiniger, E. Bucher and J. Muller, Phys. Kondens. Materie 5, 243 (1966).

105. R. Caudron, R. Caplain, J. J. Meunier and P. Costa, Phys. Rev. B8, 5247 (1973).

106. K. J. Duff and T. P. Das, Phys. Rev. B3, 192 (1971).

107. R. A. Tawil and J. Callaway, Phys. Rev. B7, 4242 (1973).

108. L. Ley, S. P. Kowalczyk, F. R. McFeely and D. A. Shirley, Lawrence Berkeley Laboratory Report No. LBL-2929, to be published in Phys. Rev. B.

109. W. Götze and P. Wölfle, J. Low Temp. Phys. 5, 575 (1971).

110. W. Götze and P. Wölfle, J. Low Temp. Phys. 6, 455 (1972).

TECHNICAL INFORMATION DIVISION
LAWRENCE BERKELEY LABORATORY
UNIVERSITY OF CALIFORNIA
BERKELEY, CALIFORNIA 94720